8-2011

Immersion Cooling of Photovoltaic Cells in Highly Concentrated Solar Beams

Ahmed Darwish
University of Nevada, Las Vegas

IMMERSION COOLING OF PHOTOVOLTAIC CELLS IN HIGHLY CONCENTRATED SOLAR BEAMS

by

Ahmed Darwish

Bachelor of Science

Al Azhar University, Cairo, Egypt

2005

A thesis submitted in partial fulfillment of

the requirements for the

Master of Science Degree in Mechanical Engineering

Department of Mechanical Engineering

Howard R. Hughes College of Engineering

Graduate College

University of Nevada, Las Vegas

August 2011

THE GRADUATE COLLEGE

We recommend the thesis prepared under our supervision by

Ahmed Darwish

entitled

Immersion Cooling of Photovoltaic Cells in Highly Concentrated Solar Beams

be accepted in partial fulfillment of the requirements for the degree of

Master of Science in Mechanical Engineering

Department of Mechanical Engineering

Robert Boehm, Committee Chair

Yi-Tung Chen, Committee Member

Suresh Sadineni, Committee Member

Aly Said, Graduate College Representative

Ronald Smith, Ph. D., Vice President for Research and Graduate Studies
and Dean of the Graduate College

August 2011

ABSTRACT

Immersion Cooling of Photovoltaic Cells in Highly Concentrated Solar Beams

by

Ahmed Darwish

Dr. Robert Boehm, Examination Committee Chair

Professor of Department of Mechanical Engineering

University of Nevada, Las Vegas (UNLV)

Concentrated solar radiation can be utilized to generate electrical power from photovoltaic cells, but concentrated solar radiation increases the photovoltaic cell's temperature. This increase in temperature can lead to degradation of the cell efficiency, and too high of a temperature can damage the cell's integrity. This is particularly important in dish and tower systems where a maximum uniform flux may be difficult to achieve. While a variety of approaches have been used to the keep the cells cool, most are based upon removal of heat from the back (opposite surface of the incident flux exposed surface) of the cell. This thesis reports on an immersion cooling technique for the cells, whereby a coolant is circulated over the front surface of the cell in addition to its other surfaces. An analysis is given where the cells are placed in a cylindrical glass tube, where a liquid is circulated. The impact of the various thermal processes that result from this approach are described herein. A comparison is made to limited experimental data.

ACKNOWLEDGEMENTS

Not enough words can express my gratitude to my advisor Dr. Robert Boehm. Dr Boehm is the solar energy godfather in the state of Nevada. Besides being open minded and an excellent teacher, he always takes care of his students and supports them during their hard times. He taught me a lot not only in the engineering point of view but also in the personal attitude, indeed working with him is a milestone in my life.

I would like to thank my committee members for their assistance and support, especially Dr. Chen for his support in the CFD modeling.

I would like to thank my CER colleagues for their continuous support, really each one of them taught me something and gave me valuable ideas and comments.

TABLE OF CONTENTS

LIST OF FIGURES

LIST OF TABLES

CHAPTER 1

1. INTRODUCTION

1.1. Basic theory of the photovoltaic cells

The photovoltaic cell is a device that converts radiation energy into electricity. Semiconductors are the material used to build these cells. When the photons fall on the surface of the photovoltaic cells, the photon energy will undergo through three main processes through which radiation energy converts to electricity. Based on these three processes, the cell efficiency can be determined [1].

The first process is the absorption of the incident radiation energy; not all photons are absorbed by the cell, since the photon has to have a certain amount of energy to be able to excite an electron to move from the valence band to the conduction band, where it can be collected as electrical current.

Fig. 1 Absorption of photon with energy $\hbar\omega$ in a semiconductor material causes excitation of an electron from the valence band to the conduction band [1].

Any photon with energy lower than the band gap energy ($\hbar\omega < \mathcal{E}_G$) cannot excite the electrons and will not be absorbed by the photovoltaic cells, it will be either reflected or transmitted. Assuming that each absorbed photon will generate one electron-hole pair, then

$$\eta_{abs} = \frac{j_{abs}}{j_{inc}} \qquad 1\text{-}1$$

where j_{abs} and j_{inc} are the absorbed and incident solar radiation respectively. The absorbed energy can be expressed as follows:

$$j_{abs} = -\frac{j_{sc}}{e}\,\hbar\omega_{abs} \qquad 1\text{-}2$$

The second process is the electron-hole pair thermalization, where the solar heat energy is converted to chemical energy. The mean energy of electron-hole pair ($\hbar\omega_{abs}$) will be reduced to $\mathcal{E}_e + \mathcal{E}_h$. As a result, the efficiency can be expressed as follows:

$$\eta_{thermalization} = \frac{\varepsilon_e + \varepsilon_h}{\hbar\omega_{abs}} = 1 - \frac{T_o}{T_s} \qquad 1\text{-}3$$

Third process is the conversion of chemical energy into electrical energy, where the electron-hole pair energy ($\mathcal{E}_e + \mathcal{E}_h$) will be converted to chemical energy (($\mu_e + \mu_h$) = eV_{oc}) as shown in equation 1-4.

$$\eta_{thermodynamic} = \frac{eV_{oc}}{\varepsilon_e + \varepsilon_h} \qquad 1\text{-}4$$

To find the maximum chemical energy; this maximum energy can be found at the open circuit conditions, but this energy will be completely dissipated with the emitted photons. The maximum power can be found at a point on the current-voltage characteristic curve for the solar cell. This curve can be found from the following equation:

$$j_Q = j_s\left[e^{\left(\frac{eV}{KT}\right)} - 1\right] + j_{sc} \qquad 1\text{-}5$$

where

$$j_s = e\, n_i^2 \left[\frac{D_e}{L_e n_A} + \frac{D_h}{L_h n_D}\right] \qquad 1\text{-}6$$

$$j_{sc} = e\, G(L_e + L_h)$$

The point of maximum power is at (V_{mp}, j_{mp}). The fill factor represents the maximum energy that can be extracted to that available as follows:

$$FF = \frac{j_{mp} V_{mp}}{j_{sc} V_{oc}} \qquad 1\text{-}7$$

The overall efficiency is the product of the three efficiencies and the fill factor

$$\eta = \frac{j_{abs}}{j_{inc}} \times \frac{\varepsilon_e + \varepsilon_h}{\hbar\omega_{abs}} \times \frac{eV_{oc}}{\varepsilon_e + \varepsilon_h} \times \frac{j_{mp} V_{mp}}{j_{sc} V_{oc}} = \frac{j_{mp} V_{mp}}{j_{inc}} \qquad 1\text{-}8$$

$$\eta = \frac{FF\, j_{sc} V_{oc}}{j_{inc}} \qquad 1\text{-}9$$

1.2. Temperature effect

Equations 1-10 to 1-13 are the semi-empirical formulas that can be used to determine the open circuit voltage, the short circuit current, and the fill factor as a function of the cell's temperature and the solar concentration ratio [2].

$$j_Q = 0.034\, a\, C\left[1 - e^{\left(\frac{V - V_{oc}}{0.026}\right)}\right] \qquad 1\text{-}10$$

$$V_{oc} = 1.25 - \left(\frac{0.63 - 0.06\, \log_{10} C}{300}\right) T \qquad 1\text{-}11$$

$$j_{sc} = 0.034\, a\, C\left[1 + 3 \times 10^{-4}(T - 300)\right] \qquad 1\text{-}12$$

$$FF = [0.8 - 0.0006(T - 300)](1 - 0.05\, C\, a\, r_s) \qquad 1\text{-}13$$

where (a) is the junction area and (r_s) is the internal series resistance (ohms).

From the above discussion we can conclude that the cell efficiency varies with both temperature and solar concentration. Different models have been proposed for the cell's

performance dependency on temperature [3], [4]. Most of these models predict the same behavior for the photovoltaic cells. The efficiency derived from these various models can be expressed in a general formula as follows [5]:

$$\eta = a_1 (1 - b_1 T_c) \qquad 1\text{-}14$$

where a_1 and b_1 are constants which depend on the PV cell material type.

1.3. PV cell operation requirements

Concentrated PV systems are usually less expensive owing to the fact that the expensive photovoltaic cell area is replaced by cheaper concentrator area such as mirrors or lenses to achieve the same power output.

Typically, high performance silicon photovoltaic cell efficiency is around 22% [6]. Solar energy concentration increases the cell's temperature and thereby reduces its efficiency [3]. Moreover, being exposed to a high temperature for prolonged time causes long term degradation of the cells [7]. A proper cooling system is required to remove that excess heat, but there are some considerations about the cooling system design, which will be discussed below.

1.3.1. Cell temperature

Besides the decrease in the cell efficiency with a temperature increase, beyond a certain temperature limit, the cell will undergo long term degradation. Usually the PV module manufacturers specify the coefficient of temperature degradation and the maximum operating temperature of the cell.

1.3.2. Cell temperature uniformity

Non-uniform temperature distribution reduces the cell efficiency [8], [9], and [10]. Usually a photovoltaic module consists of rows of cells. The rows are connected in a parallel manner, while each row consists of several cells connected in a series manner. The advantage of this series connection is the ability to increase the voltage while decreasing the current for the same output power. This decrease in current will reduce the ohmic losses. On the other hand, in series connection the current is limited by the lowest output cell. Since the cell's efficiency decreases with temperature, the cell with the highest temperature will affect the whole series connection. To overcome this problem a uniform temperature distribution along each thread connected in the series should be achieved.

1.3.3. Cooling system reliability

A reliable cooling system is a very crucial issue, since any failure in the cooling system can lead to catastrophic results from cell damage to fire hazards in extreme cases. Coolants should be selected to minimize the health and environmental hazards. A simple design can help to reduce the maintenance costs.

1.4. Cooling of PV cells under high concentration (CPV)

A high concentration of solar radiation leads to a high temperature of the cell. This increase cell temperature and the way to handle that excess heat depends on different factors such as the PV cells arrangement and the type of cooling medium.

1.4.1. Effect of concentrator geometry

The PV cell arrangement greatly affects the possible ways to handle the excess heat. In the following sections, the different concentration systems and the proper cooling techniques will be discussed.

1.4.1.1. Single PV cell arrangement

When a single cell is subjected to concentrated solar radiation, roughly the area available for cooling the cell is equal to the concentrator area as shown in Fig. 2 [5].

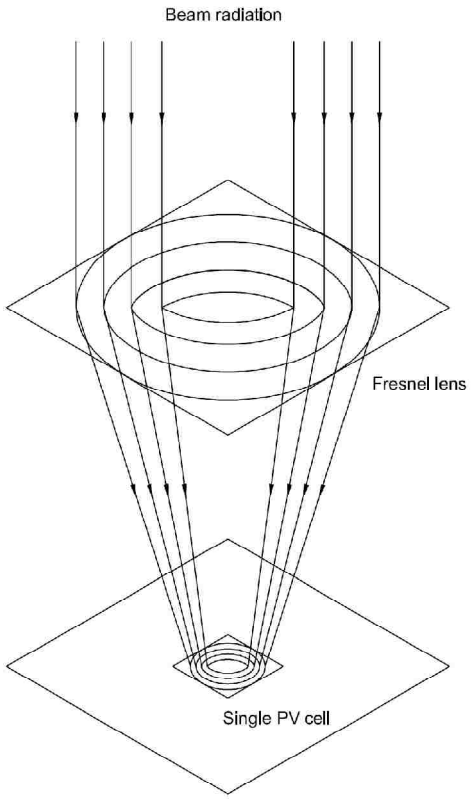

Fig. 2 Single cell arrangement.

As a result, the cell with a certain concentration ratio will have an area for cooling equal to its original area, multiplied by the concentration ratio. This arrangement allows for using passive cooling. An example of such a cooling system is the AMONIX

multi-junction cells installed at the CER where the cells are located under Fresnel lenses and cooled by natural convection from the back side.

1.4.1.2. Linear PV cell arrangement

In linear geometries, the cells are arranged in rows and subjected to concentrated solar radiation from linear concentrators such as a parabolic trough or a linear Fresnel lens. In this arrangement, each cell has less free space to dissipate the heat because it is surrounded from two sides by other cells as shown in Fig. 3. The areas available for heat rejection extend from two of the sides, front and back surfaces of the cell.

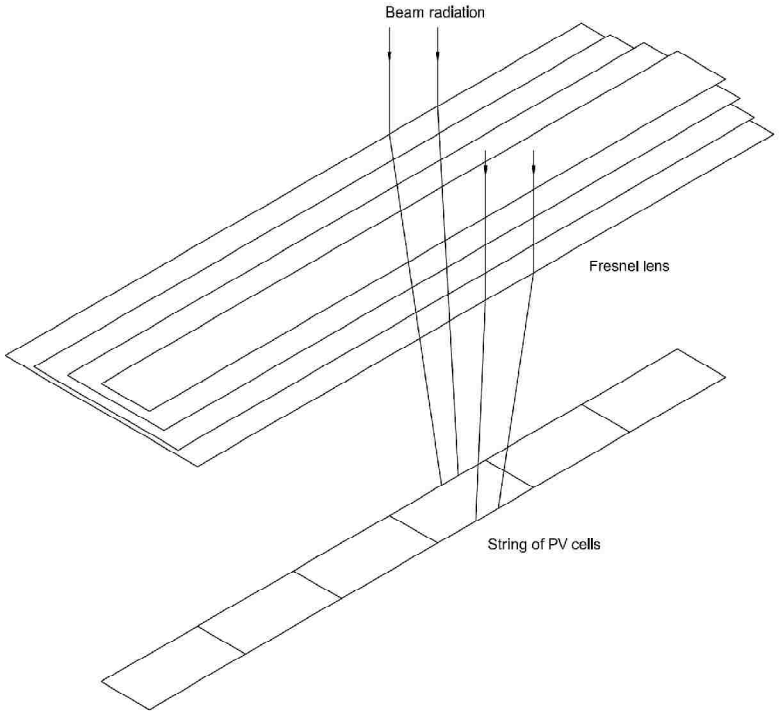

Fig. 3 Linear cell arrangement.

1.4.1.3. Densely packed PV cell arrangement

In the densely packed PV cell arrangement, each cell is surrounded by neighboring cells on four sides. Usually, this kind of arrangement is used with systems that have a large collector area and high concentration ratio such as solar dishes and heliostat

systems. Cooling of such systems is more difficult than the previous two arrangements since the heat can be dissipated only through the two normal surfaces of the cell-- the front surface and the back surface. As a result, the passive cooling is not sufficient for this arrangement with high concentration ratio and less heat dissipation area.

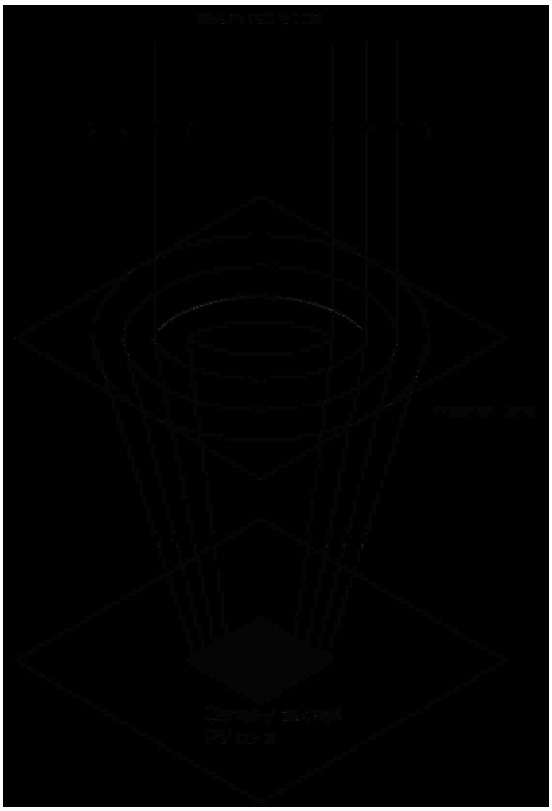

Fig. 4 Densely packed cells.

1.5. Effect of cooling medium

PV cell cooling medium should be a neutral electrolyte. The coolant will decrease the solar radiation reflection from the PV cell surface that will increase the charge carriers' concentration and also increase the carriers' life time. The PV cell coolant should also have a high dielectric constant [11]. Wang et al. [12] have studied the effect of immersing the PV cells in different liquids and found that silicon oil is stable under

ultraviolet irradiation and can be used directly for PV cells cooling. Zhu et al. [13] used the immersion cooling for densely packed PV cells, where the cells were immersed in silicon oil. In this study, a high heat transfer coefficient of 3000 W/m^2K and temperature differences of 5^o C along the cells' surface and of 1.5^o C across the cells' thickness were obtained.

1.6. CPV cooling techniques

Various cooling techniques have been proposed for cooling of solar PV cells under high concentration. These techniques aim to attain low and uniform cell temperature using simple designs. Royne et al. [14] have studied the cooling of densely packed photovoltaic cells under high concentration using a jet impingement technique. An optimization is performed for selecting the jet diameter to accommodate various cell illumination conditions. The jet cooling technique results in non-uniform heat transfer from the cells surface, although this non-uniformity didn't affect the electrical output strongly.

Passive cooling techniques are employed with linear concentrators like the trough system where the concentration ratio is low, around 20 suns. Akbarzadeh et al. [15] used a heat pipe type passive cooling system with R22 refrigerant as a cooling medium to cool down a solar trough concentrated PV system.

Using channels attached to the back of the PV cell, Lasich [16] managed to keep the cells at temperatures around 40°C. Moreover, these channels also act as a supporting structure for the PV cells. Using this design, an efficiency of 24 % has

been reported by Solar Systems Pty. Ltd. [17] where a parabolic concentrator with concentration ratio of 340 suns was used.

A densely packed PV array comprising 10 cells (6 cm × 6 cm each) subjected to concentration of 70 suns is cooled using a cold plate attached to the back of the PV array [18]. Through this cooling technique, the array efficiency reached 20.8% and the PV cell temperature is maintained at 39^{o} C.

1.7. Thesis goals and structure

This study mainly aims to analyze the concept of a new cooling technique, immersion cooling, for photovoltaic cells under highly concentrated solar radiation. The effect of the different cooling parameters on the cell performance will be investigated. Additionally, some alternatives to improve the overall system output are explored.

CHAPTER 2

2. EXPERIMENTAL SETUP

To check the validity and applicability of the proposed cooling technique, a real experimental model has been built at the Center for Energy Research (CER), UNLV. This model mainly aims to verify the concept of immersion cooling, regardless of the associated cost issues. In the following sections details of the experimental setup will be explained.

2.1. System overview

The system consists of a photovoltaic module that is enclosed in a glass pipe. The glass pipe is integrated in a cooling loop. The loop consists of a heat exchanger, a pump, and a deionizer. The glass pipe and the module are mounted in the concentration area of a dual axis tracking solar dish as shown in Fig. 5. The whole arrangement is situated at the Center for Energy Research site on the UNLV campus.

Fig. 5 SAIC Dish at CER, UNLV.

2.2. Solar concentrator and tracking system

The system under discussion consists of a two-axes tracking solar dish with nominal concentration ratio of 250 suns. The dish was built by the Science Applications International Corporation (SAIC) at UNLV to generate power from Stirling engine/generator. The dish receives the sun flux and reflects it through a matrix of mirrors on to the receiver area as shown in Fig. 5. More details about the system are explained in [19], [20].

The SAIC dish is a reflective concentrator. A steel truss structure forms the dish shape that carries 16 mirrored facets with total mirror area of 113 m^2. The structure is supported by a tubular steel pedestal. Each facet consists of flat mirror tiles (30cm by 30cm) that provide a focal area with a nominal flux distribution of approximately 250 suns. A mirror reflectance of approximately 90% is used. In case of highest solar radiation of 1100 W/m^2, the total reflected power is around 110 kW. The receiver area is around 60 cm × 60 cm.

Fig. 6 Mirror facets.

For tracking, a variable-speed drive DC motor is used. A 1.5 HP motor is used as the elevation motor, and a 1 HP motor is used as the azimuth motor.

Fig. 7 Elevation and azimuth motors.

2.3. PV module

The PV module consists of a copper substrate covered with closely packed silicon solar cells. The size of the module is approximately 5 cm by 27 cm. The module is

placed in the center of the receiver area. Due to the high concentration ratio that causes high increase in the photovoltaic cell temperature, the module is surrounded by a coolant enclosed in a transparent glass pipe. The module general specifications are summarized in Table 1.

Table 1 General Receiver Module Specifications [20].

Item	Description
Module size & shape	Rectangular, 5 cm by 27 cm
Type of photovoltaic cell	Single-crystal, back-contact Silicon
Cell size approx.	1 cm by 1 cm active area
Number of cells	88
Packing factor	94.5%
Temperature coefficient of the cells	0.25% per 1 ˚C
Receiving area	84 cm × 84 cm
Mirror reflectance	88% - 90%
Cell connection	Cells are attached to a copper plate. The front surface of the copper plate contains the circuit pattern that was formed by etching, and the cells are soldered onto this surface. [20]
Glass tube dimensions	Approximately 5.4 cm diameter × 50 cm length

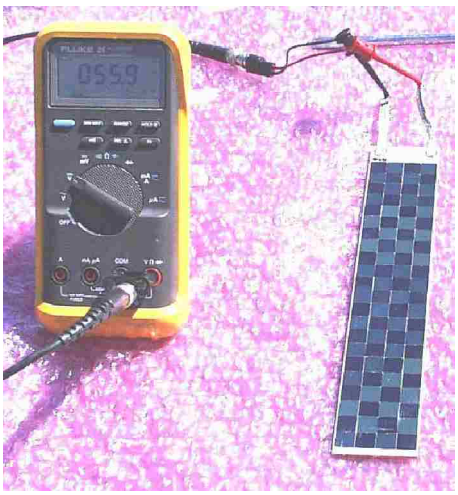

Fig. 8 Densely packed PV cells.

Fig. 9 PV module.

The extreme conditions that the module can be exposed to, for a short period without damage, are summarized in Table 2.

Table 2 Extreme module operating conditions [20].

Max. Insolation	400 kW/m^2 (400 suns)
Max. Cell Temperature	90˚C

Under the rated conditions, the module is expected to give the rated performance summarized in Table 3.

Table 3 Module rated conditions [20].

Insolation at Receiver surface	250 kW/m^2 (250 suns)
Allowable Insolation Variation at Rated Conditions	<8% from Mean
Average Cell Temperature	65˚C
Open-Circuit Voltage	72.2 V_{DC}
Output Power (peak power point)	543 W
Output Voltage (peak power point)	55.44 V_{DC}
Output Current (peak power point)	9.8 A
Design Efficiency (solar insolation on module aperture area to DC power at peak power point under rated conditions)	16.4%
Rated Efficiency Loss Rate	Less than 1 efficiency percentage point per 1000 hours of operation at rated insolation and temperature

2.4. Heat rejection system

Heat absorbed by the module is rejected by immersing the module in a dielectric cooling medium. The cooling medium should be a dielectric liquid such as deionized water or silicon oil. The cooling circulation system consists of a pump, a heat exchanger, flow meters, and piping network, which are used to form a cooling loop with the glass pipe. This active cooling system consists of two loops. The first loop is traversed by the dielectric cooling medium, which is pumped across the module by a centrifugal pump and then back to a shell and tube heat exchanger. While the second loop is traversed by the city water that exchanges heat with the dielectric cooling medium flowing through the heat exchanger.

Heat Exchanger:

A shell and tube heat exchanger is used to reject the heat from the dielectric cooling medium traversing the tube side, to the cooling water, on the shell side. The exchanger model (SSF-603-ER-1P, Young Touchstone Company) has a shell diameter of 155.4 mm and tube diameter of 9.5 mm [21].

Pump:

A centrifugal pump is used to circulate the coolant. The pump model is TE-4-MD-HC 582604 from Little Giant Pump Company. However, the city water used for the shell side of the heat exchanger is furnished the city supply pressure and doesn't need a pump.

Ion exchange column:

In case of using water as a cooling medium for the cells, the water will capture some

ions from the cells and the other metallic parts in its path. An ion exchange column is used to control the water resistivity by removing these collected ions. The water resistivity can be controlled at a certain limit of 15 MΩ cm using a bypass branch that allows some of this cooling water to go through the deionizer and return back to the main flow. The column model is OPTION-S 15BP, from ELGA LabWater Global Operations [21].

Fig. 10 Experimental set up.

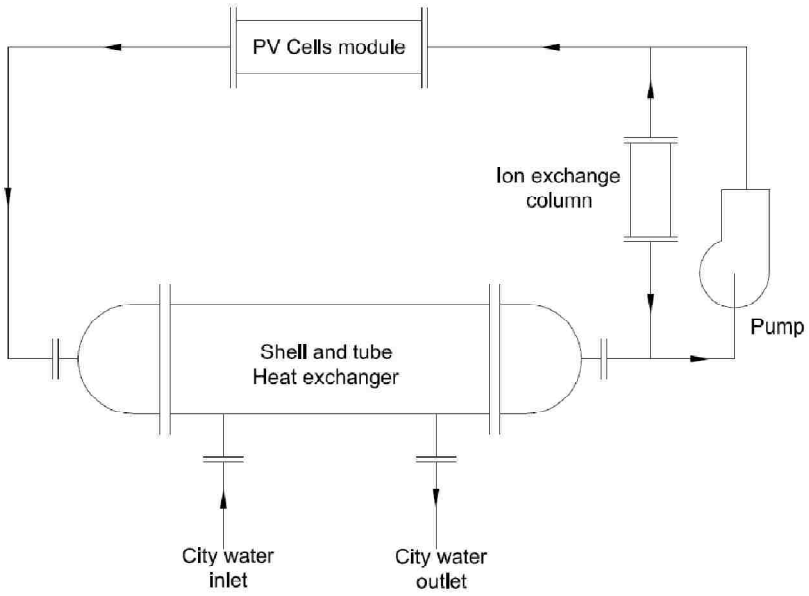

Fig. 11 Schematic drawing for the experiment

2.5. Measurements and instrumentation

The main data that needs to be collected are module temperature, mass flow rate, water resistivity and the cells' current and voltage.

A set of seven thermocouples are mounted on the back of the module to measure the temperature distribution along the substrate surface. The thermocouples models are 5TC-TT-K-36-72 or 5TC-TT-K-36-36 from the Omega company [21].

The mass flow rate is measured by a turbo flow meter (model A109GMN100NA1) manufactured by Great Plains Industries, Inc.

For the water in contact with the PV cells, an electrochemical analyzer is used to measure the water resistivity. The analyzer model 873RS-AIPFGZ is supplied by Invensys Process Systems Inc.

The current--voltage characteristic curve for the cell was collected using the tracer DC-100C, Daystar, Inc [21].

The accuracies of the above measurements are tabulated in Table 4

Table 4 Accuracies of the various instruments [21]

Measured data	Accuracy
Mass flow meter	± 1.5%, repeatability ±0.2%
Water resistivity analyzer	± 0.5%
Voltage	± 0.5% (resolution 18 mV)
Current	± 0.5% (± 45 mA with resolution of 0.3 mA).

Fig. 12 Thermocouples attached to back of the cells

CHAPTER 3

3. SYSTEM ANALYSIS

To investigate the effect of the cooling process parameters on the PV performance, an optical and thermal model is developed for the proposed system. Fig. 13 shows the electrical circuit analogy of energy exchange for the PV module. The analogy includes the thermal and the optical interactions.

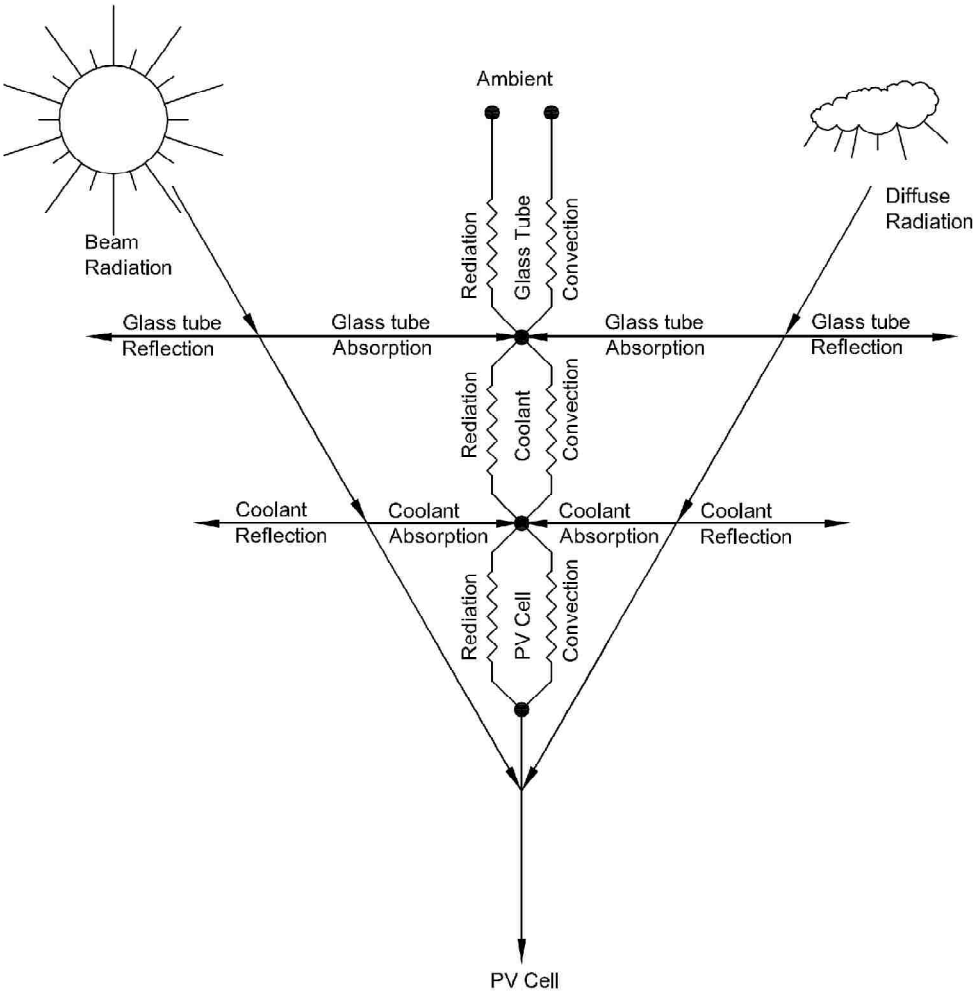

Fig. 13 The thermal circuit analog for the PV module

3.1. Optical analysis

The optical analysis includes a reflecting mirror that concentrates the sun light on to the receiver area, and the PV module. Solar radiation will have different kinds of losses due to reflection by the concentrator, and reflection and absorption by the glass tube and coolant on its path to reach the PV cell array. More details about these losses will be discussed in the following sections.

3.1.1. Concentrator

The SAIC dish mirror system is made of flat tiles instead of one smooth and continuous mirror surface. This design is favorable for two reasons: first for being easier to manufacture, assemble, maintain and even replace; second the concentration will be on a flat area instead of a focal point. This leads to a more uniform flux distribution on the receiver area.

Another advantage of the flat mirror tiles is that they can be aimed at different angles that facilitate the flux distribution control on the receiver area.

To know the amount of flux and its distribution, the SolTRACE code from NREL is used. The SolTRACE modeling results are shown in Fig. 14 where the intensity distribution on the receiver is represented in flux concentration ratio [20].

The area shown in Fig. 14 represents the receiver area of 84 cm × 84 cm where the test module with a projected area of 6 cm width × 45.72 cm length, is placed in the middle and the relevant flux can be determined accordingly.

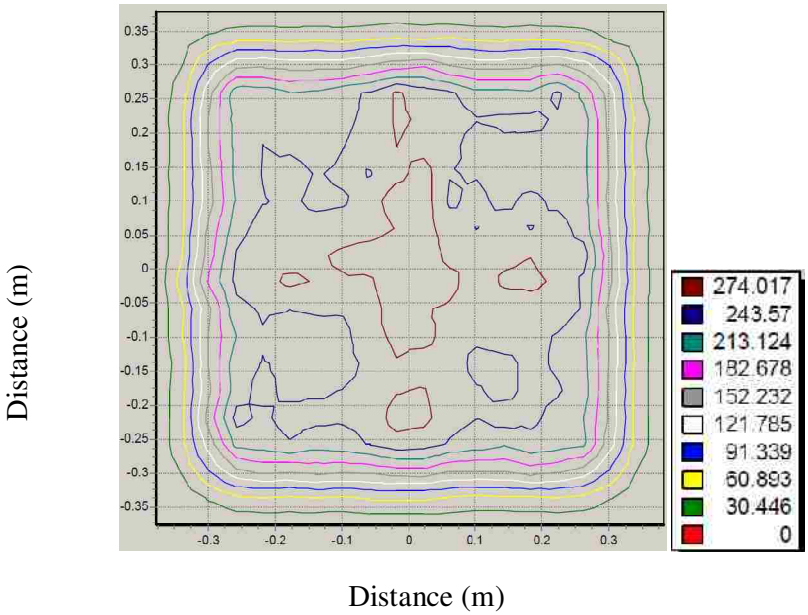

Fig. 14 Predicted flux profile for the receiver area [20].

3.1.2. PV Module (glass cover and coolant)

When the solar insolation reflects from the mirror system to the receiver through the glass tube and the coolant, it will undergo some losses due to the absorption and reflection of the rays by the glass and the cooling medium. These effects are assessed using a ray-tracing technique, shown in Fig. 15.

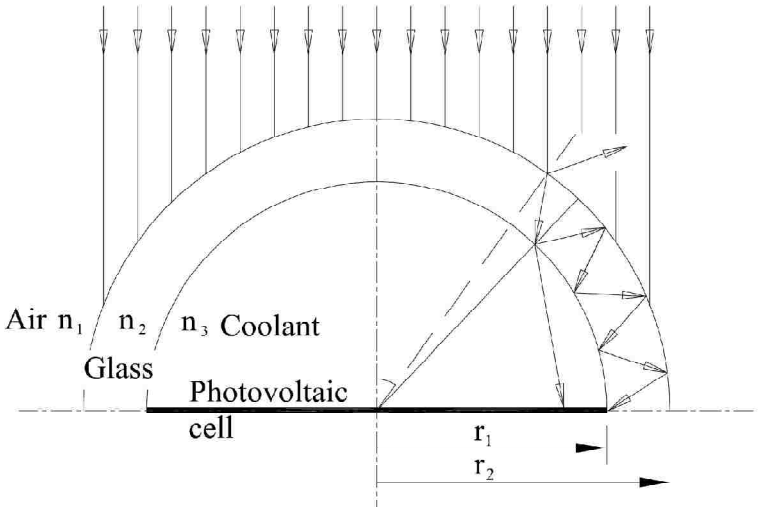

Fig 15 a

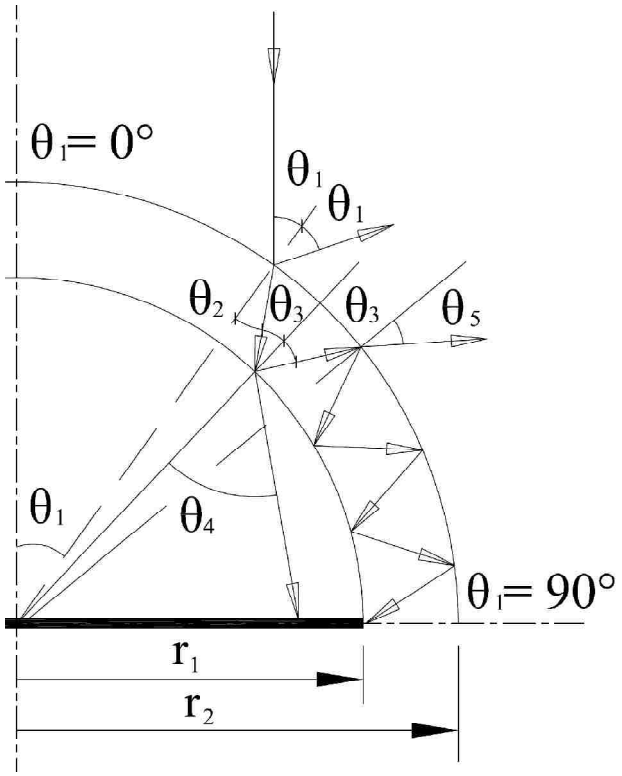

Fig 15 b

Fig. 15 Ray tracing in the glass tube a) ray bundle incident on the glass tube and b) tracing of single ray [28].

The total transmittance of the cylindrical shell and the coolant can be calculated by tracing a series of single ray paths through the cylindrical tube and through the coolant. Since the tube has a symmetric axis normal to the photovoltaic cell surface, the analysis will be applied on one half of the tube. Some of the following assumptions are applied here to facilitate the analysis. [28]

1) The concentrated beam rays are assumed normal to the cell surface, while the diffuse radiation is assumed to be normal to the tube surface, with transmittance equal to the transmittance at θ_1=0. In addition to that the diffuse radiation participation can be ignored in case of highly concentrated beam radiation.

2) Radiation is unpolarized.

3) Cell reflectance effect is neglected.

For a single ray the reflectance R_r, transmittance T_r, and absorptance A_r can be found from the following equations. [28]

$$R_r = \left[\frac{\acute{\rho}_{12} + (1 - \acute{\rho}_{12} - \rho_{12})\rho_{23}\tau_g^2}{1 - \rho_{12}\rho_{23}\tau_g^2}\right] \quad 3\text{-}1$$

$$T_r = \tau_w\left[\frac{(1 - \acute{\rho}_{12})(1 - \rho_{23})\tau_g}{1 - \rho_{12}\rho_{23}\tau_g^2}\right] \quad 3\text{-}2$$

$$A_r = \left[\frac{(1 - \tau_g)(1 - \acute{\rho}_{12})(1 - \rho_{23})\tau_g}{1 - \rho_{12}\rho_{23}\tau_g^2}\right] \quad 3\text{-}3$$

where (ρ'_{12}) is air to glass interface reflectivity, (ρ_{12}) is glass to air interface reflectivity, and (ρ_{23}) is glass to coolant interface reflectivity. The values of these reflectivities can be calculated as follows:

$$\acute{\rho}_{12} = \frac{1}{2}\left[\frac{\tan^2(\theta_1 - \theta_2)}{\tan^2(\theta_1 + \theta_2)} + \frac{\sin^2(\theta_1 - \theta_2)}{\sin^2(\theta_1 + \theta_2)}\right] \quad 3\text{-}4$$

$$\rho_{12} = \rho_{21} = \frac{1}{2}\left[\frac{\tan^2(\theta_2 - \theta_5)}{\tan^2(\theta_2 + \theta_5)} + \frac{\sin^2(\theta_2 - \theta_5)}{\sin^2(\theta_2 + \theta_5)}\right] \quad 3\text{-}5$$

$$\rho_{23} = \frac{1}{2}\left[\frac{\tan^2(\theta_3 - \theta_4)}{\tan^2(\theta_3 + \theta_4)} + \frac{\sin^2(\theta_3 - \theta_4)}{\sin^2(\theta_3 + \theta_4)}\right] \quad 3\text{-}6$$

The transmissivity of the ray through the glass is calculated as follows:

$$\tau_g = e^{[-\kappa_g(r_2\cos\theta_2 - r_1\cos\theta_3)]} \quad 3\text{-}7$$

And the transmissivity through the coolant is calculated as follows:

$$\tau_w = e^{[-\kappa_w r_1\sqrt{2}]} \quad 3\text{-}8$$

where ($r_1\sqrt{2}$) is the longest path the ray can take through the coolant, (θ_1) is the angle varying from 0^o to 90^o, and the other angles be determined by applying Snell's law. [28]

$$\theta_2 = \sin^{-1}\left(\frac{n_1}{n_2}\right) \times \sin(\theta_1) \qquad 3\text{-}9$$

$$\theta_3 = \sin^{-1}\left(\frac{r_2}{r_1}\right) \times \sin(\theta_2) \qquad 3\text{-}10$$

$$\theta_4 = \sin^{-1}\left(\frac{n_2}{n_3}\right) \times \sin(\theta_3) \qquad 3\text{-}11$$

$$\theta_5 = \sin^{-1}\left(\frac{n_2}{n_1}\right) \times \sin(\theta_2) \qquad 3\text{-}12$$

Each incident angle (θ_1) corresponds to a ray and the number of rays to be studied is decided by the value of θ_1 in the range of 0^o to 90^o.

Since no change in the reflectance, transmittance and absorptance takes place along the tube length, these properties are a function of the incidence angle only. The incidence angle changes corresponding to the radial distance along the cylindrical shell measured from the center where the plane of incidence is normal to the solar rays. The total reflectance, transmittance and absorptance can now be calculated as follows [28]:

$$R_{total} = \frac{2}{\pi}\int_{\theta_1=0}^{\theta_1=\frac{\pi}{2}} R_r(\theta_1)\, d\theta_1 \qquad 3\text{-}13$$

$$T_{total} = \frac{2}{\pi}\int_{\theta_1=0}^{\theta_1=\frac{\pi}{2}} T_r(\theta_1)\, d\theta_1 \qquad 3\text{-}14$$

$$A_{total} = \frac{2}{\pi}\int_{\theta_1=0}^{\theta_1=\frac{\pi}{2}} A_r(\theta_1)\, d\theta_1 \qquad 3\text{-}15$$

Equations (3-13) to (3-15) were used to determine the hemispherical spectral transmittance for the combination of the glass tube and the cooling water. To calculate the total transmittance, the absorption coefficients of water for different wave lengths

are used. Table 5 shows the absorption coefficient for three wavelengths in the visible region for water [29].

Table 5 Absorption coefficient of water [29].

Wavelength λ, μm	κ_λ, cm^{-1}
0.4	0.00058
0.55	0.000045
0.7	0.0060

Solar radiation reflected from the photovoltaic cell surface can be ignored. This is because the reflected energy will be trapped by the low glass transmittance for this wavelength range. Total transmittance is calculated for different wavelengths and is averaged. Fig. 16 shows the change in the transmittance with the incidence angle (θ_1).

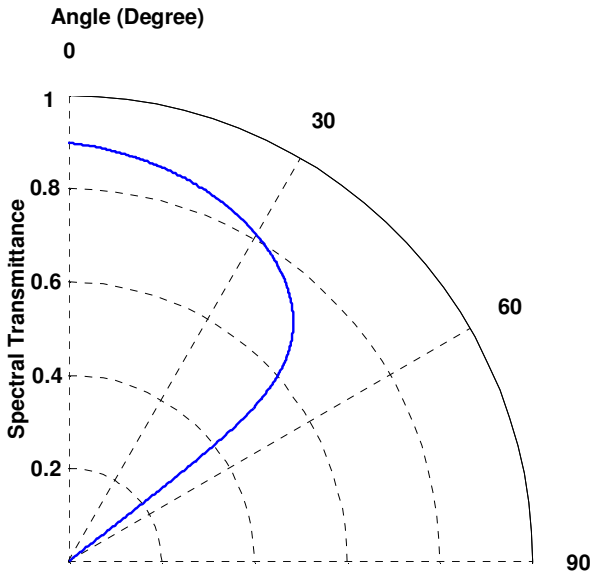

Fig. 16 Transmittance change with angle which corresponds to the distance through the glass that the ray travels at wavelength of 0.55 μm.

Fig. 17 shows the hemispherical spectral transmittance for the combination of the glass tube and the water. Superimposing this transmittance on the solar irradiance at 1.5 air mass (AM). Fig. 18 shows that most of the solar radiation spectrum will be transmitted except that part in the infrared that will be absorbed by the water. This infrared region of the solar spectrum is not benefitial for the PV cells for electricity generation, but it will increase the cell temperature and reduce the electricity output of the PV cell.

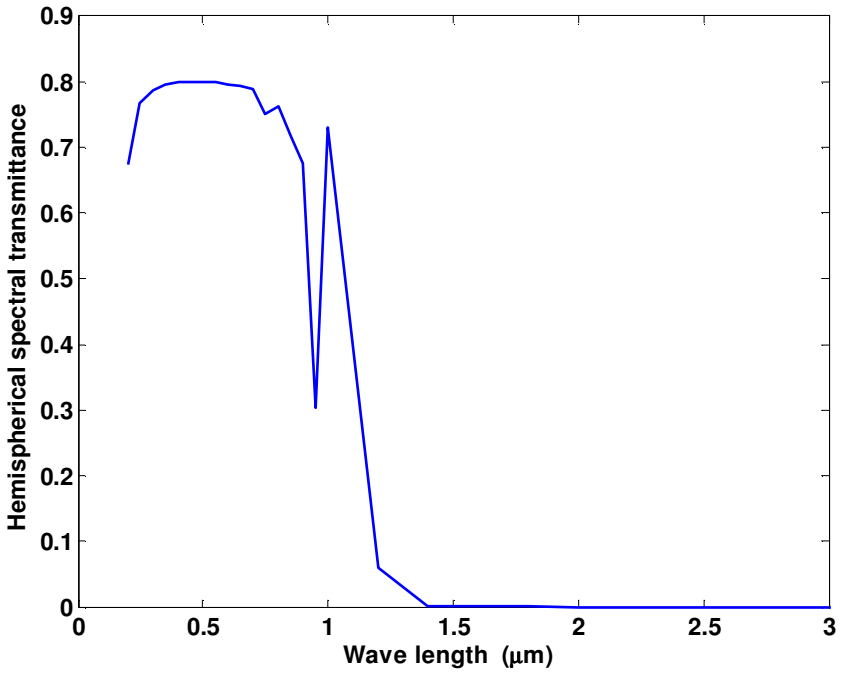

Fig. 17 Hemispherical spectral transmittance for the combination of the glass tube and water.

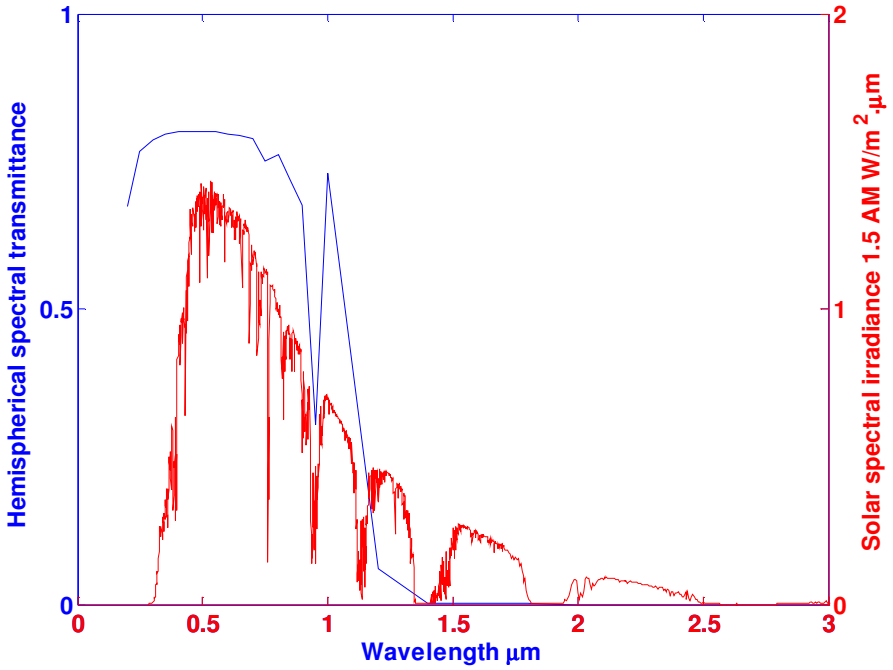

Fig. 18 Transmittance and solar irradiance at 1.5 AM.

3.1.3. Ray tracing code validation

A model is developed using a commercial ray tracing code to determine the transmittance of the composition of the glass tube and the coolant as shown in Fig. 19. The transmittance resulting from the ray tracing and the commercial code were compared at different angles of incidence. Comparative results show a good agreement for incident angles ranging from zero to around 50°. The model in the study is subjected to rays at 0° incident angle, but various incident angles are considered to show the impact of the analysis approach.

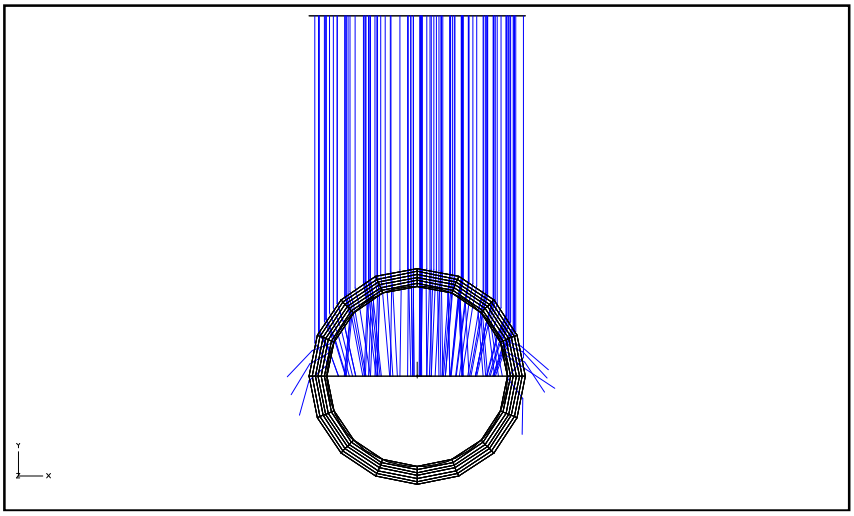

Fig 19 a

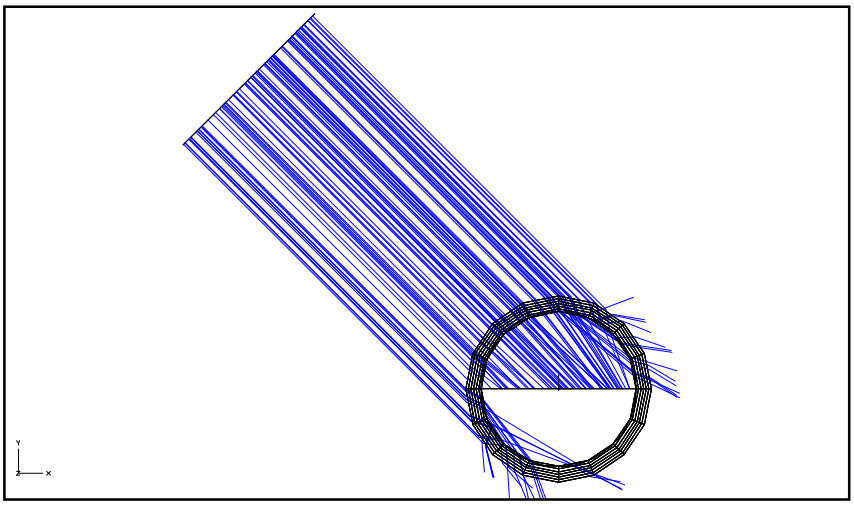

Fig 19 b

Fig. 19 The commercial ray tracing code model. a) 0^{o} incidence angle, b) 45^{o} incidence angle.

A ray tracing code using MATLAB is also developed. The results of the MATLAB code and the commercial code are compared as shown in Fig. 20. The difference at higher incident angles is of minor importance for the present application. Both the results match closely for angles between 0° and 50°, the application range.

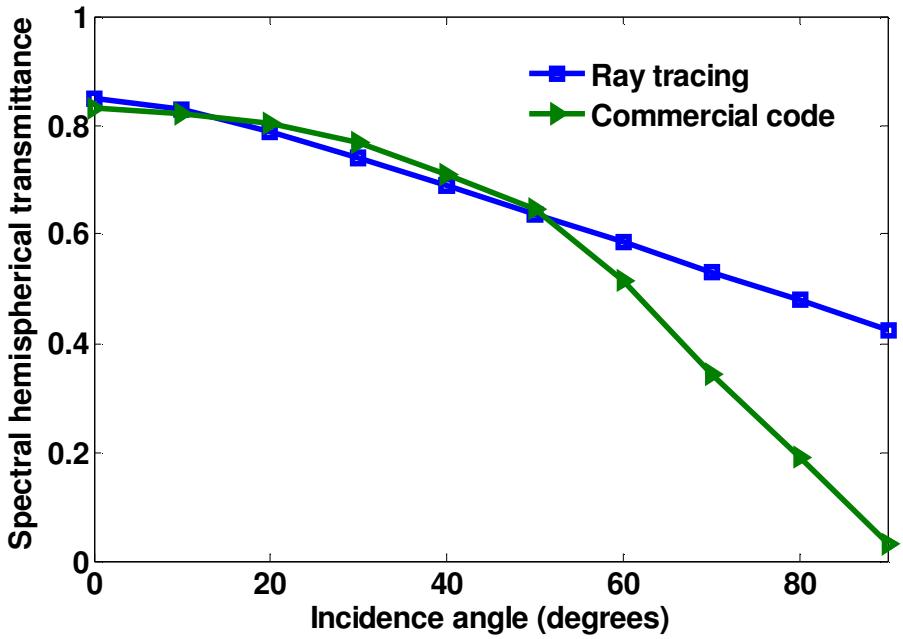

Fig. 20 Effect of the incidence angle on the transmittance, with comparison between the ray tracing results and the commercial code results.

3.2. Thermal analysis

The tube can be considered as a body with two concentric semi cylindrical surfaces, while the module consists of photovoltaic cells attached to a copper plate with a small thickness of 3 mm. This is placed at the center of the glass tube. The module absorbs the solar radiation and is considered as a heat source inside the cylinder. Contact between the cell and the cylindrical tube is ignored, so no conduction heat transfer will take place between the module and the cylindrical shell. The power output from the cell and its efficiency are temperature dependent. In order to find the cell temperature a simple thermodynamic analysis is applied on the whole system.

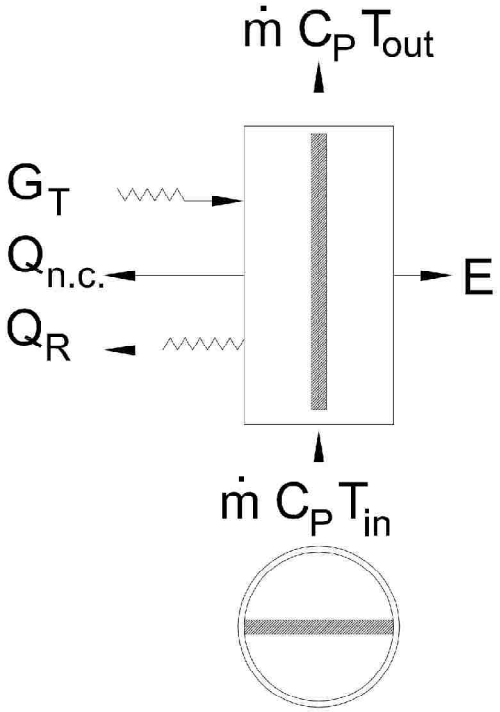

Fig. 21 The energy balance on the PV cells array and the glass tube.

The heat balance on the glass wall is applied, assuming no temperature gradient within the glass thickness. The glass wall is subjected to concentrated solar radiation some of this radiation is absorbed by the glass, but most of it is transmitted. The glass wall dissipates heat by natural convection and radiation to the ambient air at the external interface, and by forced convection to the coolant at the internal interface.

The heat transfer by radiation ($Q_{R.1}$) and natural convection ($Q_{n.c.1}$) from the glass tube to the ambient is expressed as follows:

$$Q_{R1} = \sigma \varepsilon_g A_{g.ext} \left(T_g^4 - T_\infty^4 \right) \qquad 3\text{-}16$$

$$Q_{n.c.1} = h_{n.c.} A_{g.ext} \left(T_g - T_\infty \right) \qquad 3\text{-}17$$

where the natural convection heat transfer coefficient is approximated as follows [30]:

$$h_{n.c.} = 5.7 + 3.8\, V \qquad 3\text{-}18$$

while the heat transfer by forced convection from the glass tube to the coolant is expressed as follows:

$$Q_{f.c.1} = h_{f.c.} A_{g.int} \left(T_g - T_m \right) \quad 3\text{-}19$$

where

$$T_m = \frac{T_o + T_i}{2} \quad 3\text{-}20$$

and the forced convection heat transfer coefficient is calculated using the following equation: [31]

$$h_{f.c.} = Nu_D \frac{\kappa}{D_h} \quad 3\text{-}21$$

The Colburn correlation (equation 3-22) for fully developed turbulent flow in a channel is used to obtain the Nusselt number used in equation 3-21 to determine the heat transfer coefficient [31], [33].

$$Nu_D = 0.023 \, Re_D^{\frac{4}{5}} \, Pr^{\frac{1}{3}} \quad 3\text{-}22$$

However, for cells near the inlet, fluid entrance effects must be taken into account. If the ratio of the distance from the inlet (L) to hydraulic diameter (D_h) is between 10 and 400, the following correlation is used [31], [33]:

$$Nu_D = 0.036 \, Re_D^{\frac{4}{5}} \, Pr^{\frac{1}{3}} \left(\frac{D}{L} \right)^{0.055} \quad 3\text{-}23$$

where

$$Re_D = \frac{4 \dot{m}}{(2r_1 + \pi r_1)\mu} \quad 3\text{-}24$$

$$D_h = \frac{2\pi}{(2 + \pi)} r_1 \quad 3\text{-}25$$

The heat transfer coefficient ($h_{f.c}$). values obtained from the above equations are sufficiently accurate for most Photovoltaic/Thermal applications [2].

The total heat balance on the glass tube is as follows:

$$Q_{R.1} + Q_{f.c.1} + Q_{n.c.1} = A_{g.pro} H_b A_{total} M + A_g H_d \alpha_g \quad 3\text{-}26$$

The coolant will receive heat from the absorbed solar radiation, the module surface, and the glass surface. The heat transferred to the coolant by forced convection from the glass tube and the module respectively are:

$$Q_{f.c.1} = h_{f.c} A_{g.int} M(T_g - T_m) \quad 3\text{-}27$$

$$Q_{f.c.2} = h_{f.c} A_{pv}(T_{pv} - T_m) + h_{f.c.} A_p(T_p - T_m) \quad 3\text{-}28$$

where the forced convection heat transfer coefficient is calculated as shown before in equations (3-21 to 3-25). The heat gained by absorption of solar radiation is expressed as follows:

$$Q_{R.2} = A_{g.pro} H_b A_{total} M + A_g H_d \tau_g \alpha_w \quad 3\text{-}29$$

where the module is subjected to beam radiation along the projected area and diffuse radiation on the total glass pipe area. The total heat balance on the coolant is expressed as follows:

$$Q_{R.2} + Q_{f.c.1} + Q_{f.c.2} = \dot{m} C_p (T_o - T_i) \quad 3\text{-}30$$

The module consists of a photovoltaic cell array that is attached to a copper plate. Since the thicknesses of the cell and the copper plate are small, the heat transfer from the edges will be ignored. Heat transfer by conduction will take place between the two parts.

$$Q_{pv-in} = A_{pv} \kappa_{pv} \left(\frac{T_{pv} - T_{in}}{t_{pv}} \right) \quad 3\text{-}31$$

$$Q_{in-p} = A_p \kappa_p \left(\frac{T_{in} - T_p}{t_p} \right) \quad 3\text{-}32$$

No contact resistance is assumed, and the interface temperature (T_{in}) is considered the same for the cell and the copper plate. Any radiation losses from the cell surface are ignored. Since the temperature of the cell is low, any resultant emitted radiation falls under the long wavelength category which is trapped by the low transmittance glass cover. The heat gained due to solar radiation can be expressed as follows:

$$Q_{R.3} = A_{pv}\left(H_b T_{total} \alpha_{pv} M + H_d \tau_g \tau_w \alpha_{pv}\right) \quad 3\text{-}33$$

where T_{total} is the total transmittance of beam radiation through the glass pipe and the coolant. α_{pv} is the cell absorptivity, and τ_g and τ_w are the glass and water transmittance for the diffuse radiation respectively. Heat transferred by forced convection from the two sides of the module is given by equation (3-34).

$$Q_{f.c.3} = h_{f.c.} A_{pv}\left(T_{pv} - T_m\right) + h_{f.c.} A_p\left(T_p - T_m\right) \quad 3\text{-}34$$

Although, the coolant temperatures on the two sides of the tube are different leading to different heat transfer coefficients, the temperature difference is small that the heat transfer coefficient is assumed equal on both sides.

The electrical power can be expressed in terms of the temperature of the cell as follows [32]:

$$E = \eta_{T_{ref}} Q_{R.3} \tau_{pv}\left[1 - 0.0045\left(T_{pv} - 25\right)\right] \quad 3\text{-}35$$

The heat balance on the module, consisting of the photovoltaic cells and the copper plate, is expressed as follows:

$$Q_{R.3} = E + Q_{f.c.3} \quad 3\text{-}36$$

where $Q_{R.3}$ is determined by applying the heat balance on the photovoltaic cell only. This is expressed as follows:

$$Q_{R.3} = Q_{pv-in} + h_{f.c.}A_{pv}(T_{pv} - T_m) + E \qquad 3\text{-}37$$

Similarly, the heat balance on the copper plate is expressed as follows:

$$Q_{in-p} = h_{f.c.}A_{pv}(T_p - T_m) \qquad 3\text{-}38$$

Using the above analysis the effect of the change of the coolant mass flow rate on the cell performance is determined while keeping the other experimental conditions fixed. The following figures (Fig. 22) depict the change in various performance parameters with the change in coolant mass flow rate. The power output of the module does not include the parasitic losses.

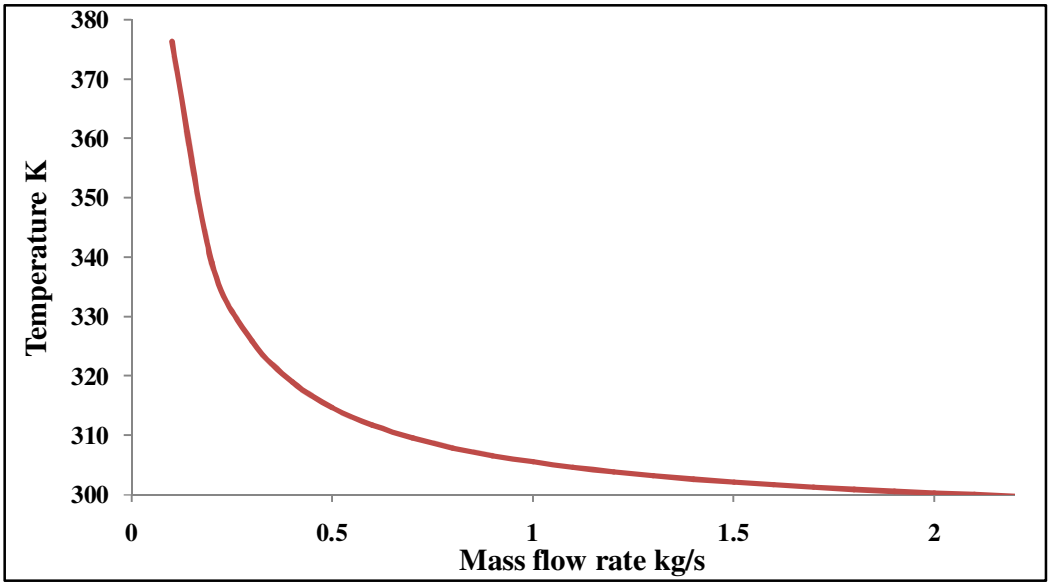

Fig 22 a

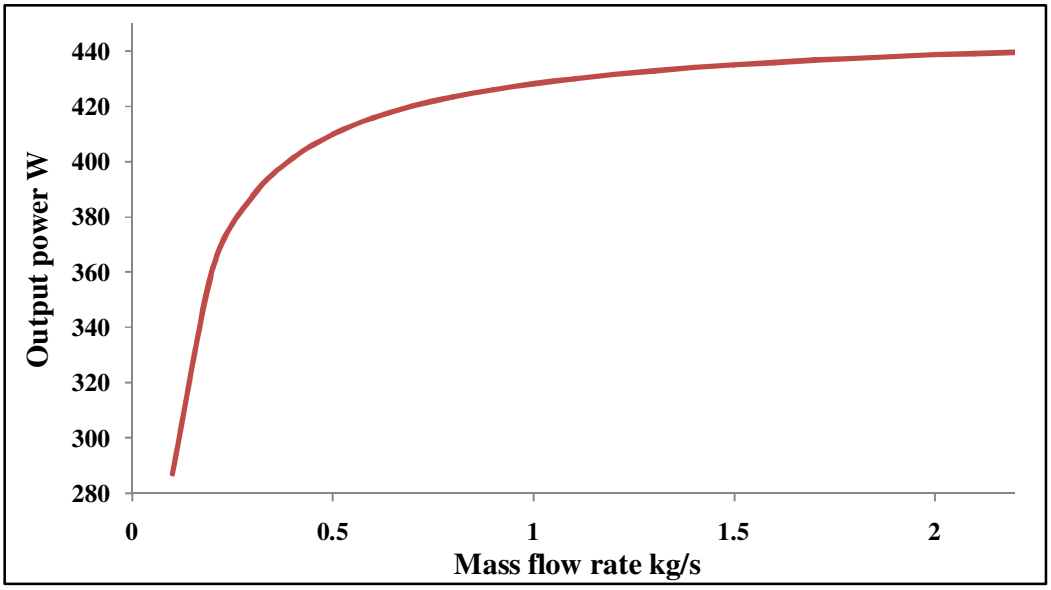

Fig 22 b

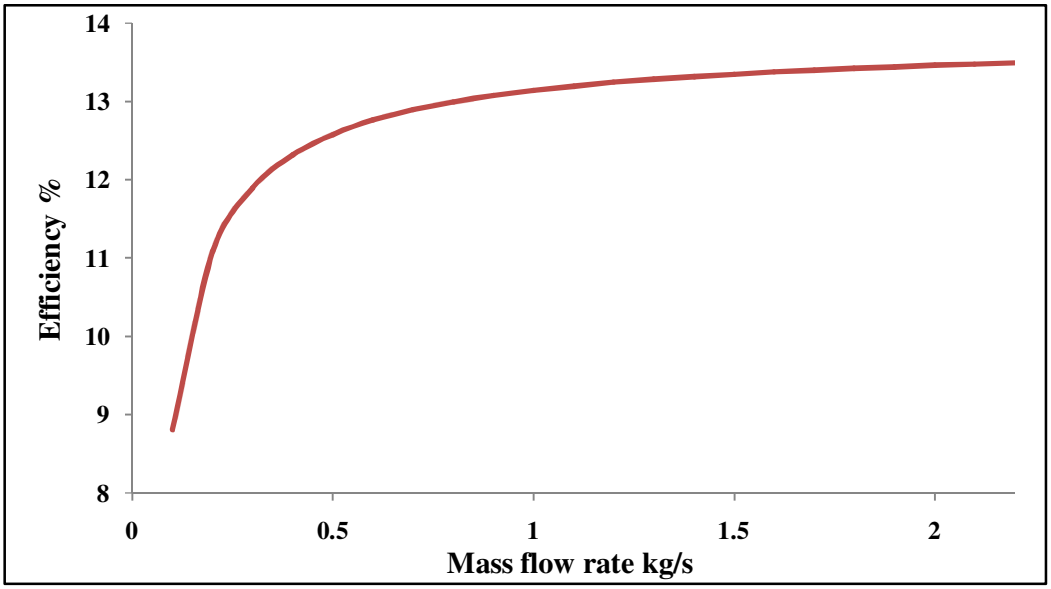

Fig 22 c

Fig. 22 The flow rate dependency for a) Cell temperature, b) Output power, c) Efficiency.

3.3. Parasitic loss

Only a part of the parasitic losses are represented in the form of the pressure drop in the glass pipe. The parasitic losses in the glass pipe are shown in Fig. 23. These

losses increase owing to the usage of sun tracking and with the increase in the mass flow rate (pumping losses). An optimization between the power gain and the parasitic loss has to be considered. Since the parasitic losses change with the tilt angle, the worst case scenario of 90° tilt angle should be considered. Fig. 24 shows that the increase in mass flow rate can increase both the power output and the parasitic losses.

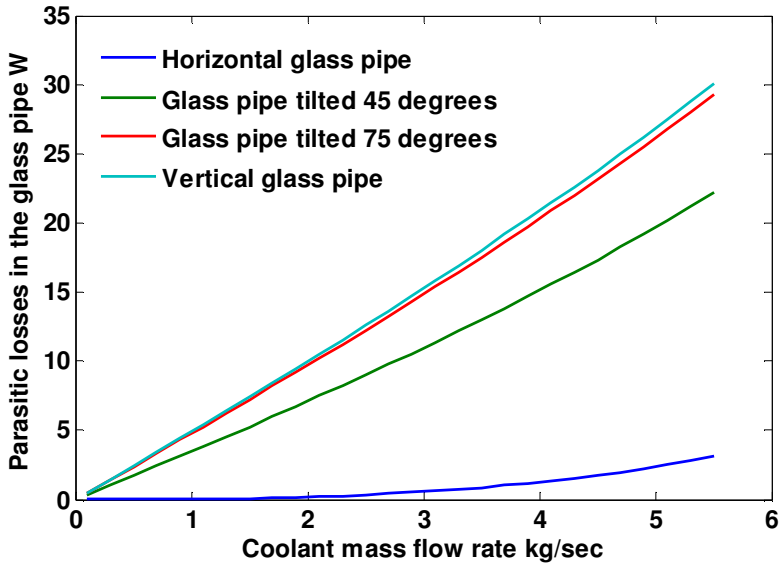

Fig. 23 The parasitic losses in the glass pipe.

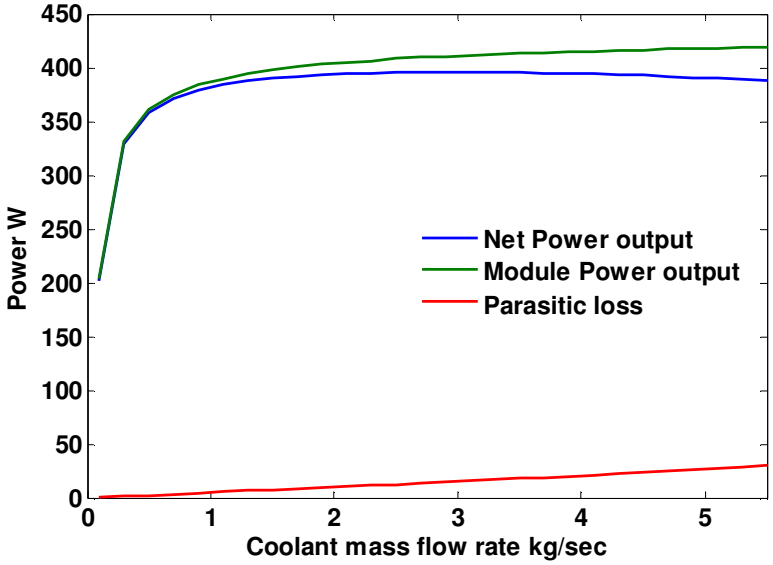

Fig. 24 Net power output.

3.4. CFD Analysis

In the previous thermal analysis, the forced convection heat transfer coefficients are assumed to be constant as indicated by the Colburn correlation in equations 3-22, and 23. As a result, the temperature determined from this analysis is constant along the PV module surface. In order to have a good estimation for the temperature distribution, a CFD model is developed using Fluent program. The model uses the advantage of the symmetry in the glass pipe to reduce the computing time to one fourth of the original computing time.

3.4.1. Assumptions and boundary conditions

The model consists of a copper substrate inside a glass tube and surrounded by water as shown in Fig. 25. Besides the symmetry assumption, several assumptions were done to simplify the Fluent analysis. These assumptions can be summarized as follows:

1- Since the silicon cells have a small thickness (less than 1 mm) and thermal conductivity around 145 W/mK, which is more than one third that of the copper, the thermal resistance of silicon can be ignored and the model will consider only the copper substrate.

2- The heat transfer by convection from the outer glass surface is calculated using equation 3-18.

3- The heat gained from the solar radiation is assumed to be heat generation in the copper substrate after considering the reflection and absorption losses.

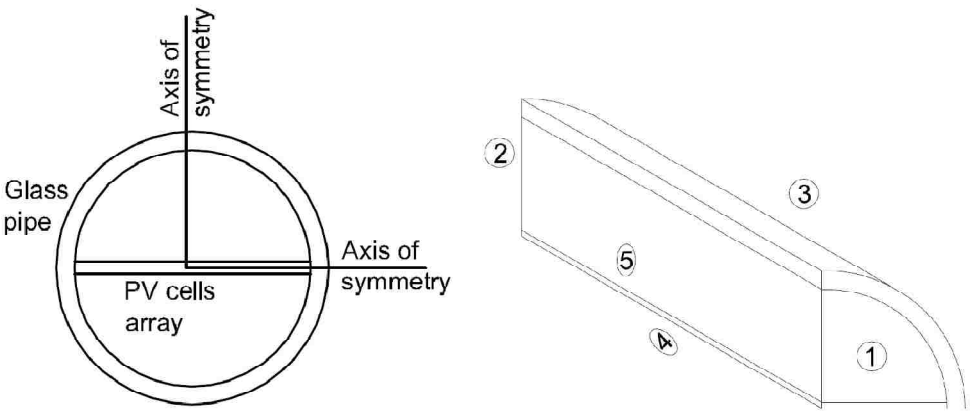

Fig. 25 Model and the axis of symmetry.

The boundary conditions for the model are summarized in Table 6:

Table 6 Summary of the boundary conditions

Face No.	Face Type	Magnitude
1	Inlet mass flow rate	0.625 kg/s, 300 K
2	Outlet pressure	1 atm
3	Convection heat transfer	14 W/m^2K (estimated from equation 3-18 at wind speed of 2.1 kg/s)
4	Symmetry wall	No heat or mass transfer
5	Symmetry wall	No heat or mass transfer

3.4.2. Computer modeling and meshing

The model is built using the SolidWorks design program with the same actual dimensions mentioned before in chapter 2. The CAD drawing output is exported to Gambit program for meshing. The mesh contains 2714827 cells and 551334 nodes. A

finer mesh size is selected for the boundary fluid-solid interface and coarser for the rest of the domain as shown in Fig. 26.

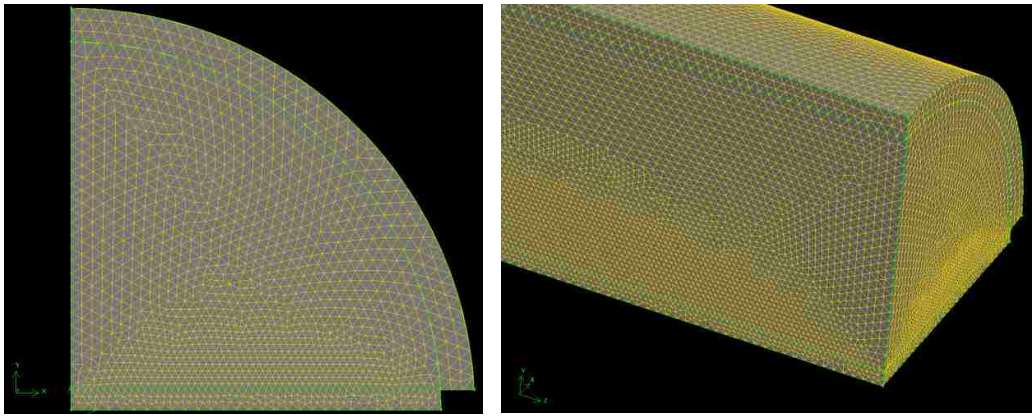

Fig. 26 Smaller mesh size at the fluid/solid interface.

3.4.3. Mesh independent study

To check the solution dependency on the mesh size, two arbitrary points in the computational domain were selected and the solution was done for different mesh size. The points coordinates are A (0.14 mm, 1.5 mm, 0 mm) and B (15 mm, 0 mm, 180 mm)A Comparison between the solutions at the these points for different mesh sized is summarized in Table 7

Table 7 Mesh independency study

Max element size at the solid / liquid interface (mm)	No. of elements	T@ A (K)	Error %	T@ B (K)	Error %
1	1665885	331.3	-	339.8	-

0.8	1915927	326.9	2.21	332.3	1.3 %
0.5	2714827	326.1	1.3	327.7	0.25 %

Table 7 shows that mesh size of 0.5 mm size can be used in modeling the PV module with sufficient accuracy.

3.4.4. Results and discussion

The mesh is exported from Gambit to Fluent program. After setting the domains, the boundary conditions, and compiling the problem the following distributions are obtained after the solution is converged.

3.4.4.1. Temperature distribution

As expected the temperature is not uniform as assumed before. The lowest temperature value is at the entrance while the highest is at the exit.

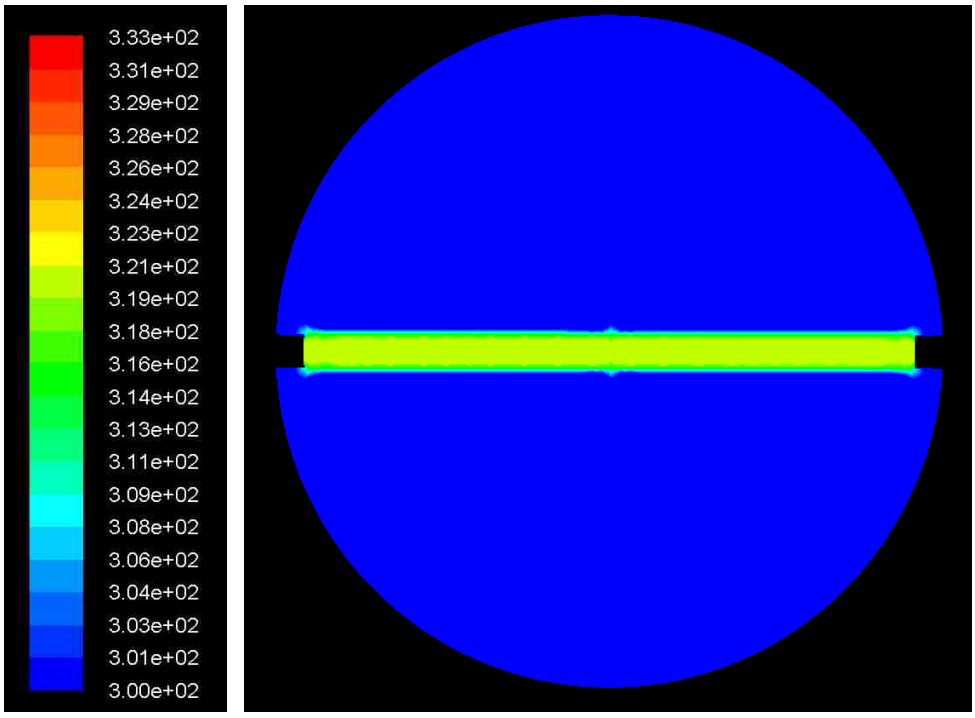

Fig. 27 Temperature distribution at the entrance (K).

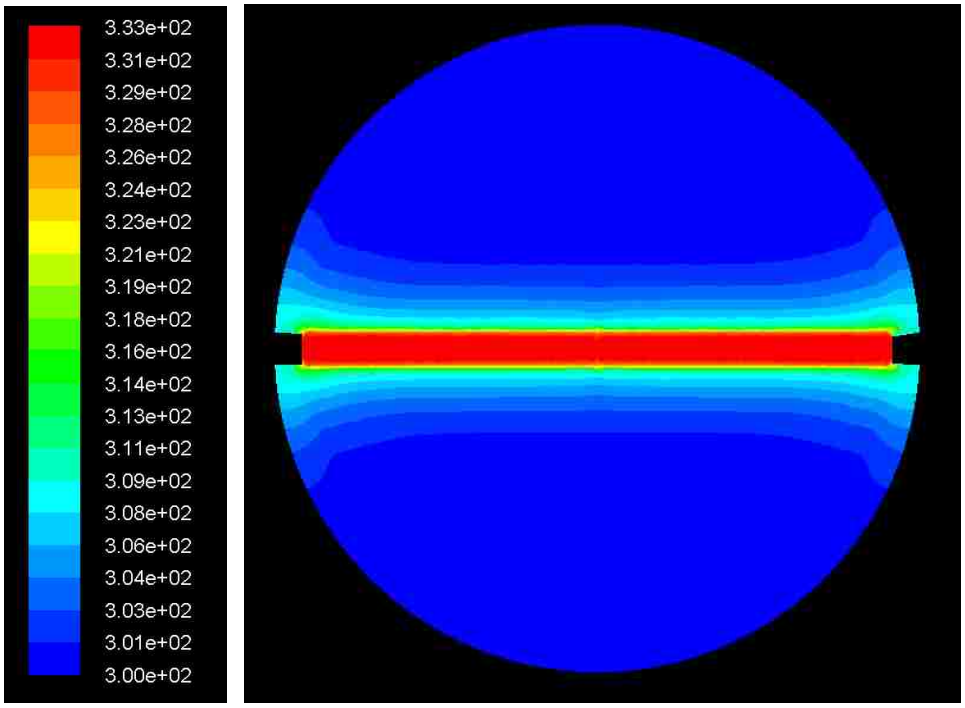

Fig. 28 Temperature distribution at the exit (K).

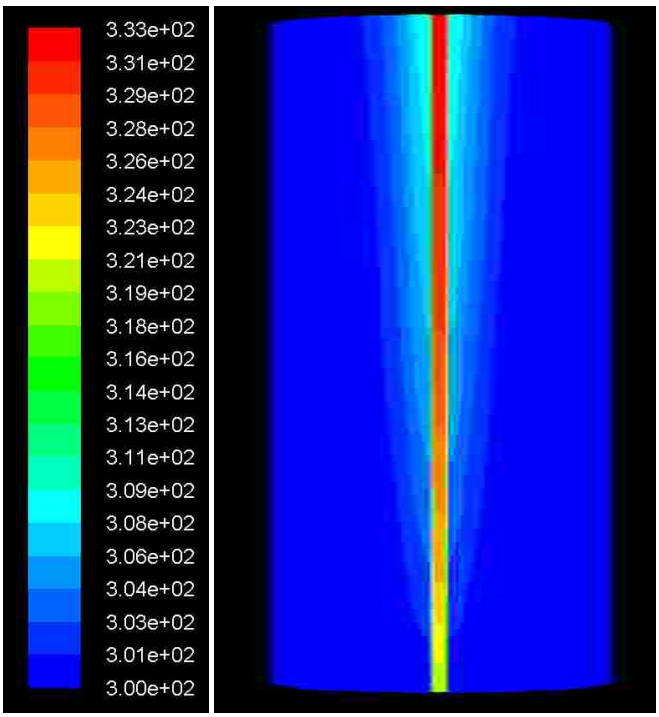

Fig. 29 Temperature distribution along the module (K).

Fig. 30 shows the main goal of the model which is the temperature uniformity along the PV cells array that varies from around 318 K to 333 K.

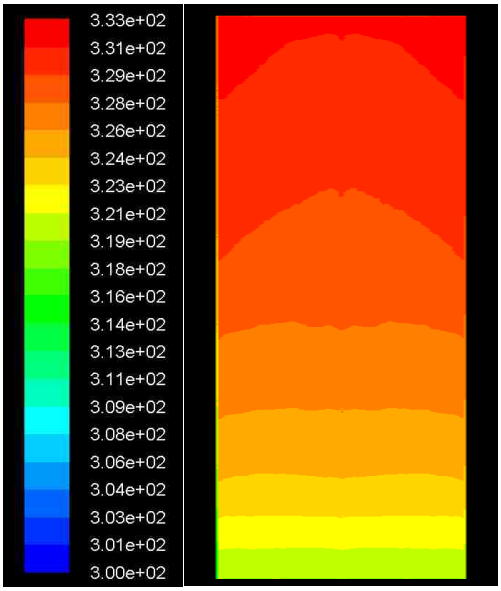

Fig. 30 Temperature distribution along the PV cells array (K).

3.4.4.2. Heat transfer coefficient and velocity distributions

The magnitude and distribution of the heat transfer coefficient are a representation of the effectiveness of the cooling process. The heat transfer coefficient along the PV cells array changes from around 2000 W/m^2K to 3600 W/m^2K.

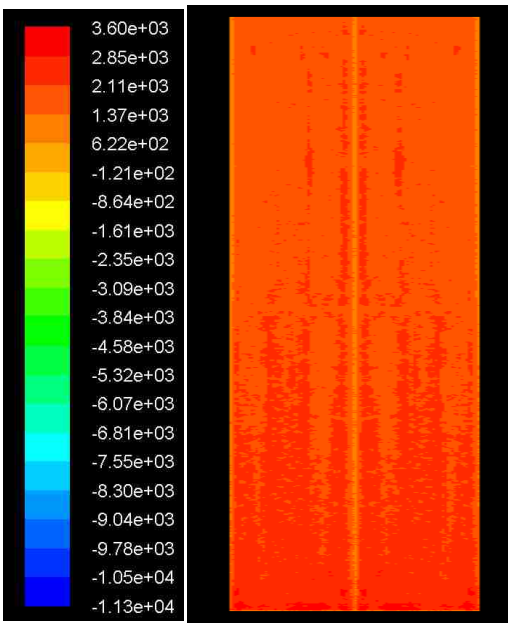

Fig. 31 Heat transfer coefficient distribution along the PV cells array (K).

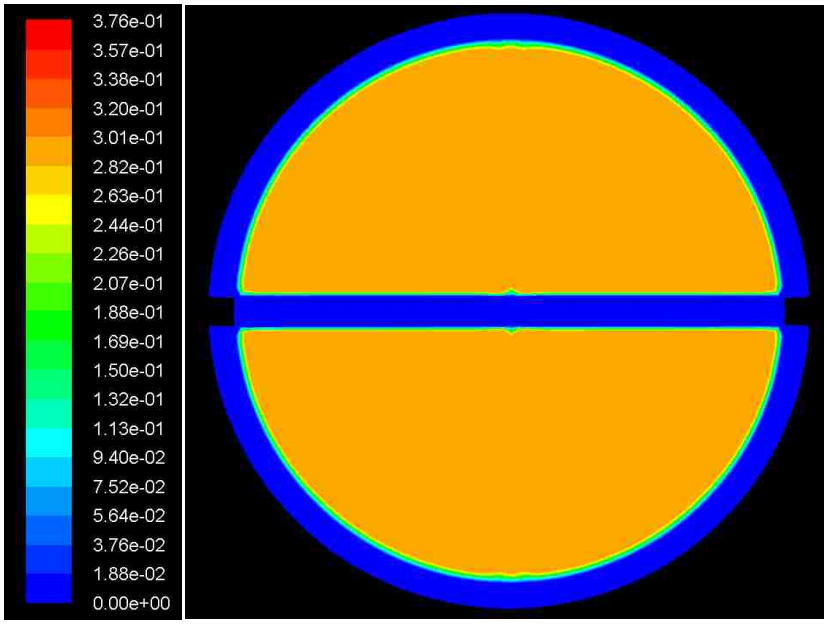

Fig. 32 Velocity distribution at the entrance section (m/s).

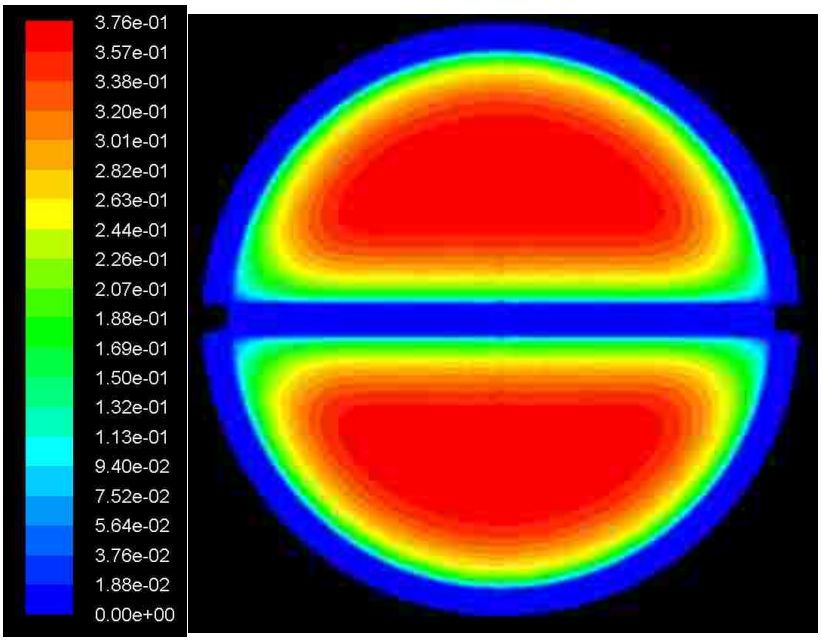

Fig. 33 Velocity distribution at the exit section (m/s).

The above model shows non-uniformity in the heat transfer coefficient and temperature distributions. This non-uniformity can affect the PV cell array output. The maximum temperature and the maximum temperature difference expected from the model are around 333 K and 15 K respectively. The experimental measurements for the same conditions show corresponding values of 318 K and 10 K respectively. The simplified thermal analysis yields a fixed heat transfer coefficient of 3578 W/m^2K and a uniform temperature of 321 K under the same experimental conditions.

CHAPTER 4

4. RESULTS AND DISCUSSION

To check the performance of the PV cell under immersion cooling, the system was operated for several days from 10 AM to 12:30 PM. Temperature, voltage, current, and direct normal incidence (DNI) data is collected. Deionozed water and silicon oil were used as coolants in two different sets of experiments.

4.1. Experimental conditions and results

Two sets of experiments are performed using two different cooling mediums. The experimental conditions for the two sets are summarized in Table 8.

Table 8 Summary of the experimental conditions

Coolant type	Water	Silicon oil
Average coolant mass flow rate	0.625 kg/s	1.833 kg/s
Average coolant inlet temperature	30 ^{o}C	44.7 ^{o}C
Average ambient temperature	20 ^{o}C	25.64 ^{o}C
Average wind speed	2.1 m/s	2.1 m/s
Concentrating mirror reflectivity	88% - 90%	88% - 90%
Total tube and coolant transmittance	0.8	0.75
Cell reference efficiency	25% at 25 ^{o}C	25% at 25 ^{o}C

Immersion cooling should fulfill two goals. First is to attain a low operating

temperature and second is to have a uniform temperature distribution. Fig. 34 and Fig. 35 show the average cell temperature change with DNI for immersion cooling using deionized water and silicon oil respectively. While Fig. 36 and Fig. 37 show the maximum temperature difference along the PV module.

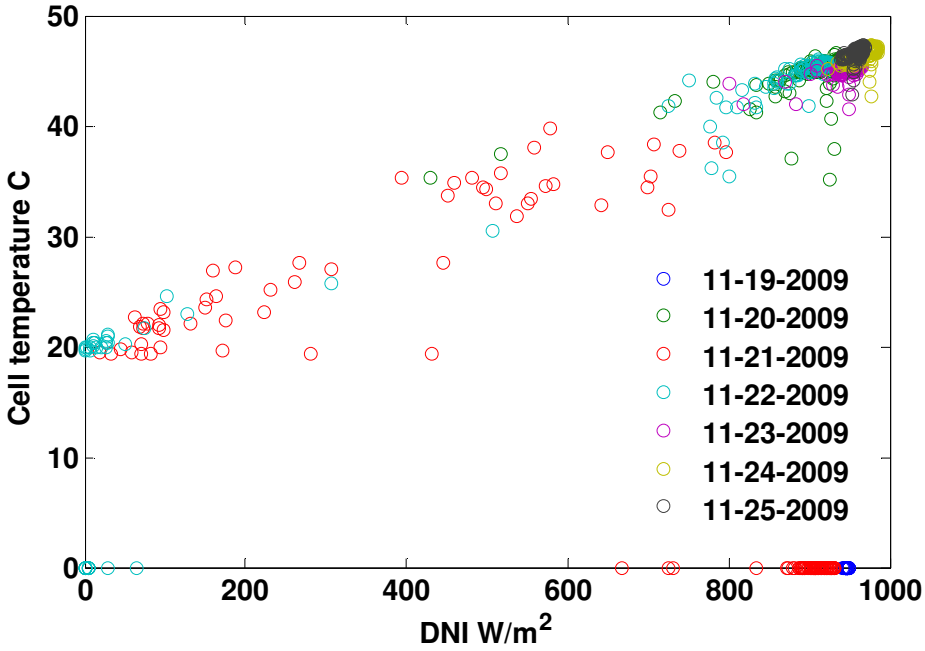

Fig. 34 Cell temperature dependency on DNI for deionized water cooling.

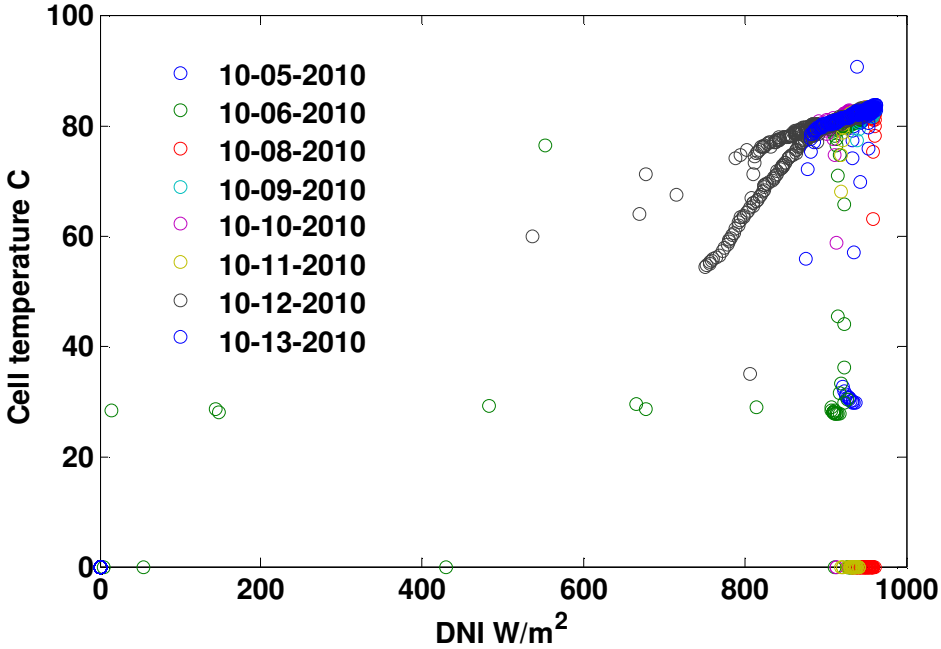

Fig. 35 Cell temperature dependency on DNI for silicon oil cooling.

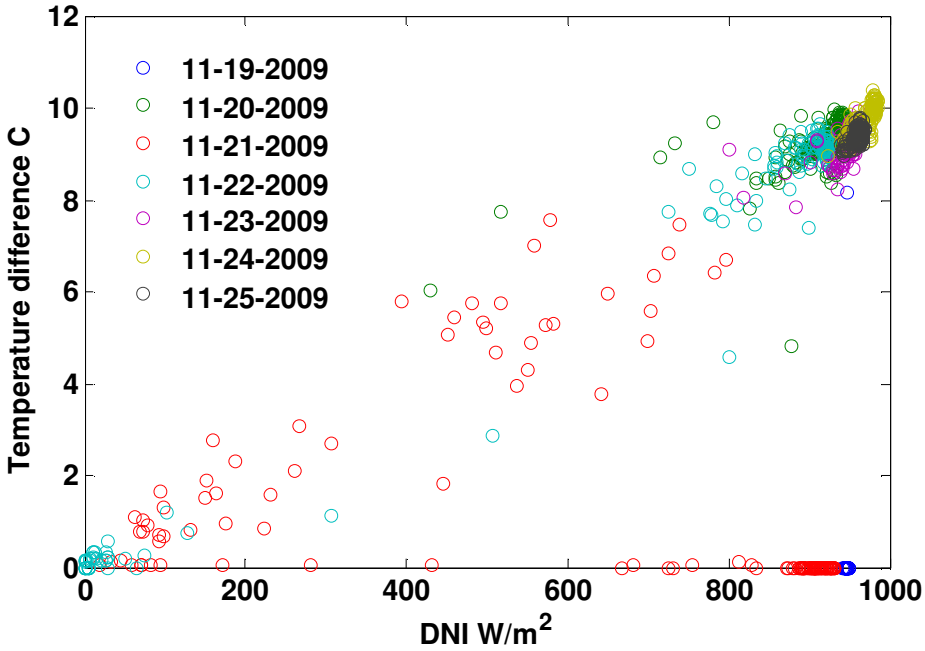

Fig. 36 Cell temperature difference for deionized water immersion.

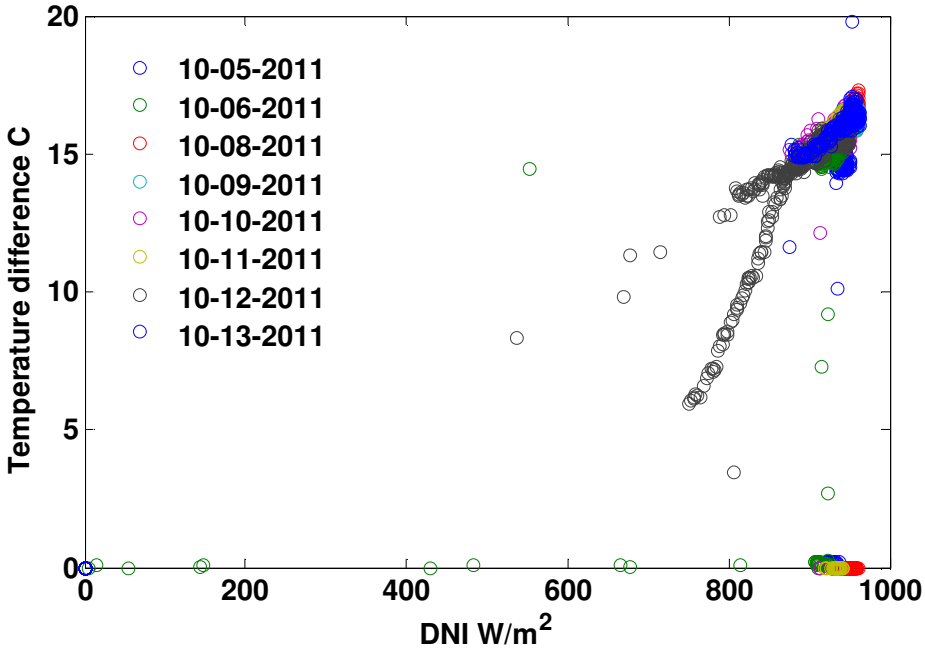

Fig. 37 Cell temperature difference for deionized water immersion.

The above graphs show the advantage of using the water as a coolant since it can maintain the PV cell at lower temperatures than the silicon oil. Comparatively, water immersion cooling provides better temperature uniformity along the PV module

surface than silicon oil. Additionally, the pumping requirements for water are lower than that for silicon oil due to lower mass flow rate required and smaller viscosity of water. On the other hand, using water requires a deionizer to maintain the water at high resistivity values which is not required for the silicon oil. It is noticed that degradation in the cell output occurs with time in the case of water immersion. This degradation can be caused by the accumulation of ions in the adjacent boundary layer to the cell since this boundary layer has small or zero velocity. Fig. 38 and Fig. 39 show the output power for the two cooling mediums.

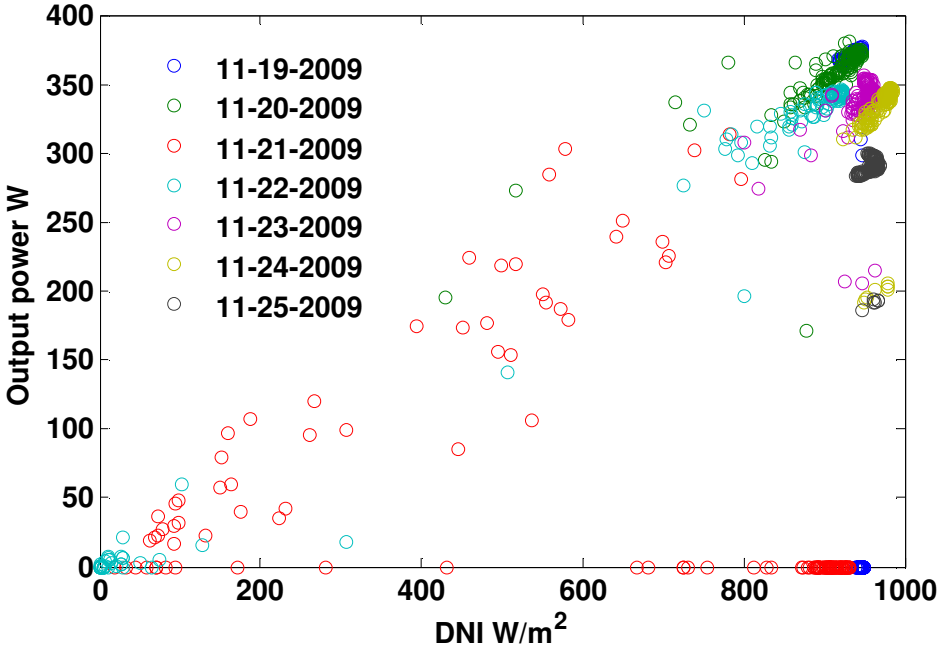

Fig. 38 Output power dependency on DNI for deionized water cooling.

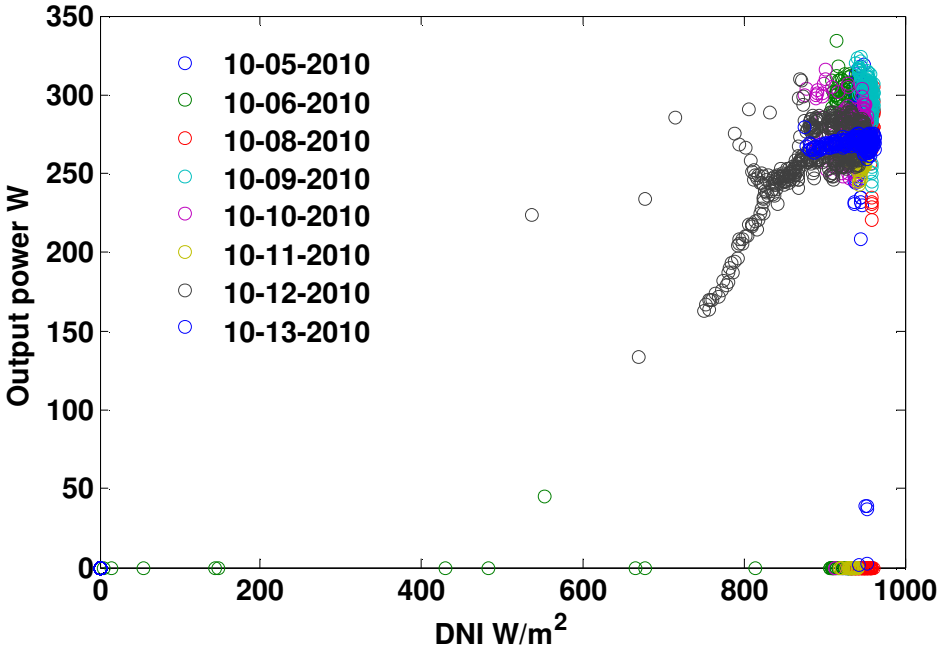

Fig. 39 Output power dependency on DNI for silicon oil cooling.

4.2. Comparison between the analysis results and the measured data

The main purpose of this experiment is to study an effective way of cooling the module and the effect of temperature on the module performance. To validate the proposed optical and thermal analysis it is compared with the experimental results. As a result a computer code is written to solve the equations (3-26, 3-30, 3-36, 3-37, and 3-38) simultaneously. This code can be used to examine different coolants at different operating conditions for yearlong performance using TMY3 data.

The code addresses the effect of solar radiation and coolant flow rate on the power output of the module without including the parasitic losses. The parasitic losses in this experiment include the power required to circulate the coolant through the piping and the heat exchanger, and it also includes the power required for SAIC dish control and tracking systems. Since the study of the module is particularly concerned with the fundamentals of this cooling technique, the net power output of

the module is relatively small in comparison to the parasitic losses, especially the tracking power. Fig. 40 to Fig. 43 compare the code results and the corresponding experimental results.

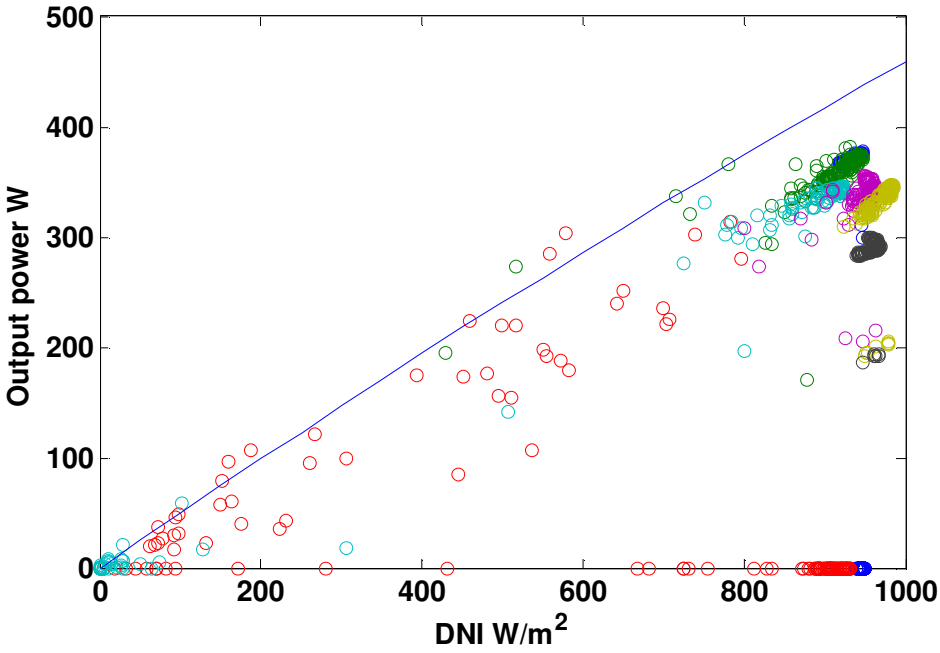

Fig. 40 Power output versus DNI for measured data (circles) and calculated data (line) in case of deionized water.

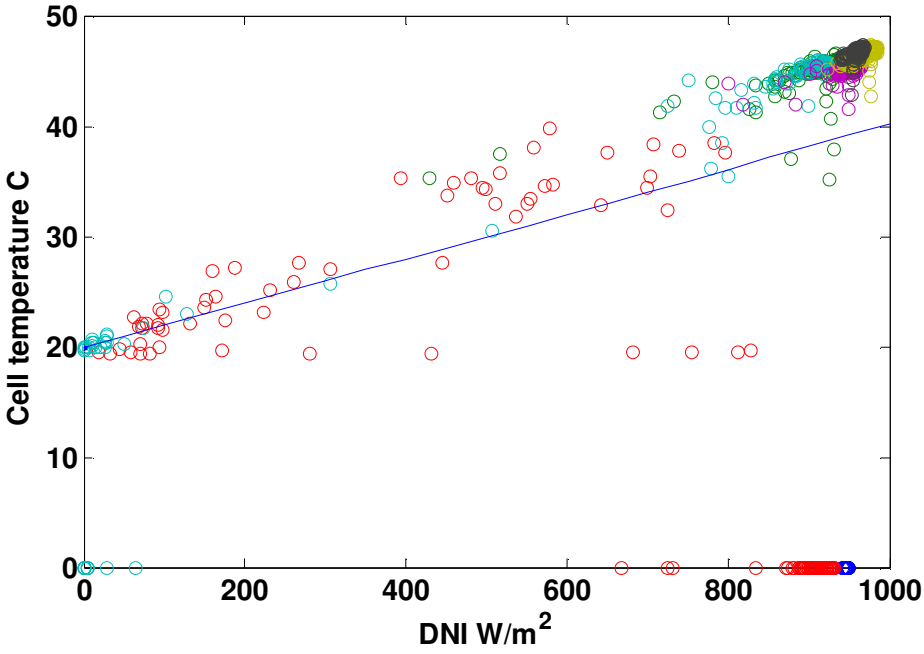

Fig. 41 Cell temperature versus DNI for measured data (circles) and calculated data (line) in case of deionized water.

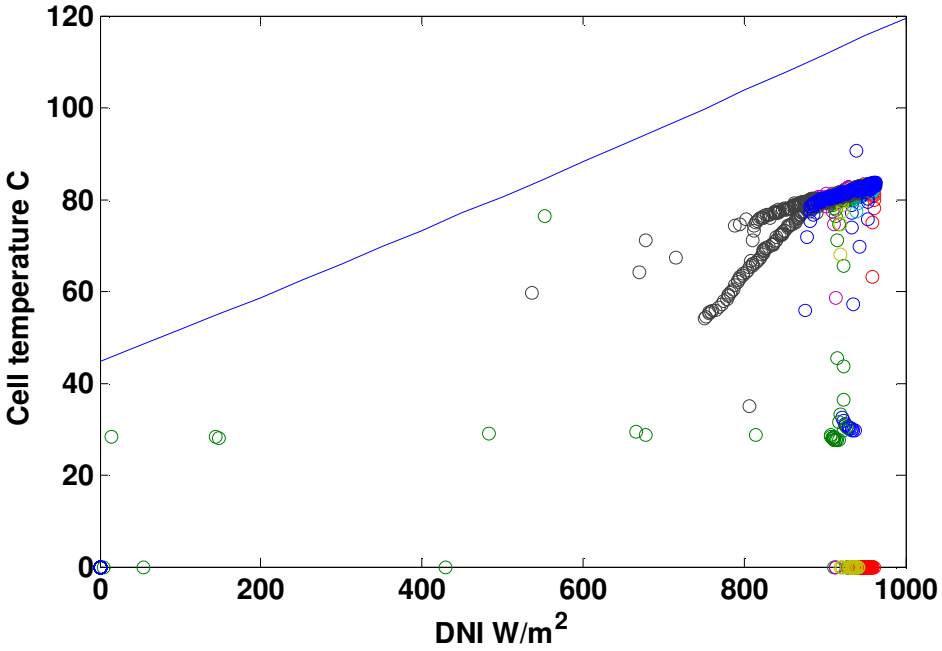

Fig. 42 Cell temperature versus DNI for measured data (circles) and calculated data (line) in case of silicon oil.

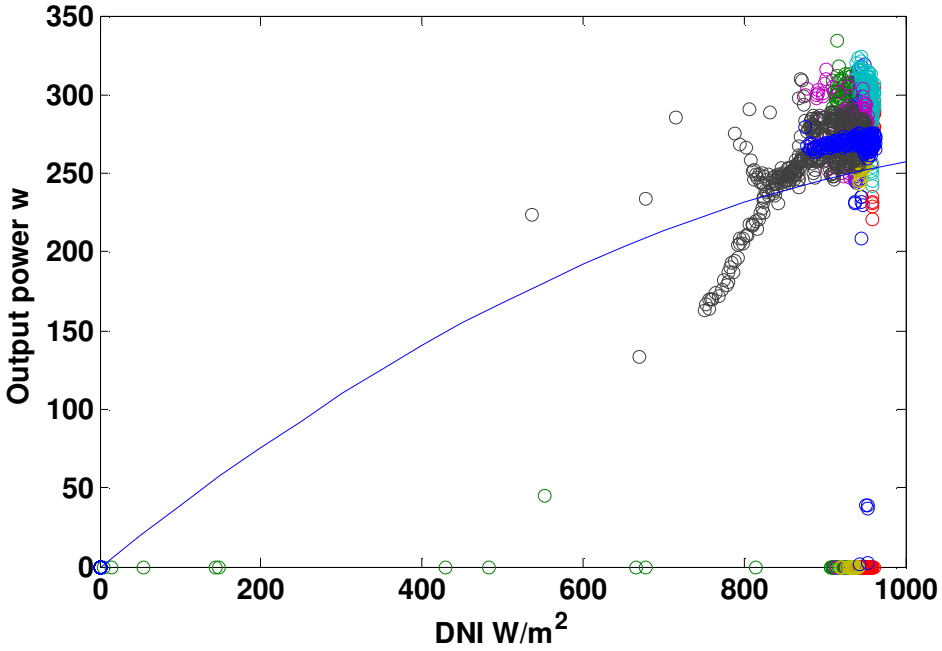

Fig. 43 Power output versus DNI for measured data (circles) and calculated data (line) in case of silicon oil.

Fig. 40 shows the electrical power output of the module versus the DNI based on the data collected through several experimental runs under the test conditions shown

in Table 8. Using a regression analysis, the relationship between the power output and the DNI can be studied. The correlation analysis for electrical power output and DNI shows that the correlation coefficients are equal or close to 1 which means that a strong positive linear relationship exists between the data.

Using the least square method, the following relationship between the power output and the DNI is obtained.

$$P = 0.4 \times DNI - 7.3 \qquad 3\text{-}39$$

Fig. 40 also shows the calculated values from the computer code. Calculated output power has the same trend of the measured data with higher values that can result from assuming uniform normal solar flux of 250 suns on the module. Of course, in reality the flux is not uniform as shown in Fig. 14, and not exactly normal. This non-uniformity and misalignment have not been considered in this analysis.

A quantitative comparison between the measured data and the code results has been done by testing the null hypothesis (H0) verses the alternative hypothesis (H1) for the measured and the calculated output power with a significance level of 0.05, where

H0 : mean calculated output power = mean measured output power

H1 : mean calculated output power ≠ mean measured output power

The statistical data for the measured and calculated power are summarized in Table 9. Since the significance level is 0.05 and the Levene's test shows p-value of 0.475, the equal variance t-tests can be used to test the hypothesis.

Table 9 Summary of the statistical data

Data	Calculated power	Measured power
Number of data points	184	184
Mean	333.94	321.47
Standard deviation	93.995	88.973
Standard error Mean	6.929	6.559

The independent t-test results with 366 degrees of freedom indicates that there is no significant difference between the mean value of the measured output power and the mean value of the calculated output power. Here the resulting p-value of 0.192 is higher than the significance level of 0.05, and the resulting t-value is 1.307. Table 10 summarizes the results of the Levene's test and the independent t-test.

Table 10 Summary of the tests results

Levene's test for equality of variances	F	0.503
	Significance level	0.479
t-test for equality of means	t	1.307
	Degrees of freedom	366
	Significance level (2-tailed)	0.192
	Mean Difference	12.474
	Standard Error Difference	9.541
	95% Confidence interval (Lower)	-6.289
	95% Confidence interval (Upper)	31.237

The percentage of error in the calculated output power to the measured output power can be found by subtracting the mean value of the measured power from the mean value of the calculated power and dividing by the mean value of the measured power that gives an error of 4 %. More experimental data points should be collected to have a more accurate validation for the computer code. Also more experimental work should be done at different mass flow rates and using different coolants to check the code validity at these conditions.

CHAPTER 5

5. SYSTEM IMPROVEMENTS

The main purpose of the proposed system is to test the concept of immersion cooling for the PV cells and to prove it. For the system to be commercially feasible, it has to undergo some improvements. These improvements should include the different parameters in the process as well the concentration system used.

5.1. Container design

Using a circular tube as a container for the cooling medium has the advantage of being easily integrated in the piping system, but usually a large concentration area is available and in such cases the glass pipe arrangement will not be convenient. In case of having larger concentration area, the photovoltaic cells can be placed in a rectangular container with a flat glass window. The flat glass window has the advantage of constant transmittance along its surface area, which helps to have a more uniform solar radiation on the module surface as shown in Fig. 44. Non-uniformity in the solar flux can reduce the efficiency of the cell matrix as mentioned in the first chapter.

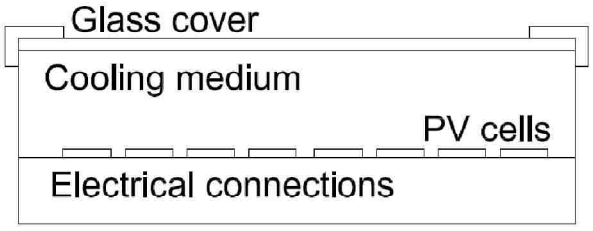

Fig. 44 A model of the rectangular container for the PV cells and the cooling medium.

To find a start point for the rectangular container design; first the total area of the cells is calculated based on the concentration area provided by the dish as shown in Fig. 45. The area available for the SAIC solar dish is enough for 24 modules similar to that one under study. Secondly the fluid inlet area has two dimensions, length and height, the length is also well defined as mentioned before, but the height should be carefully selected.

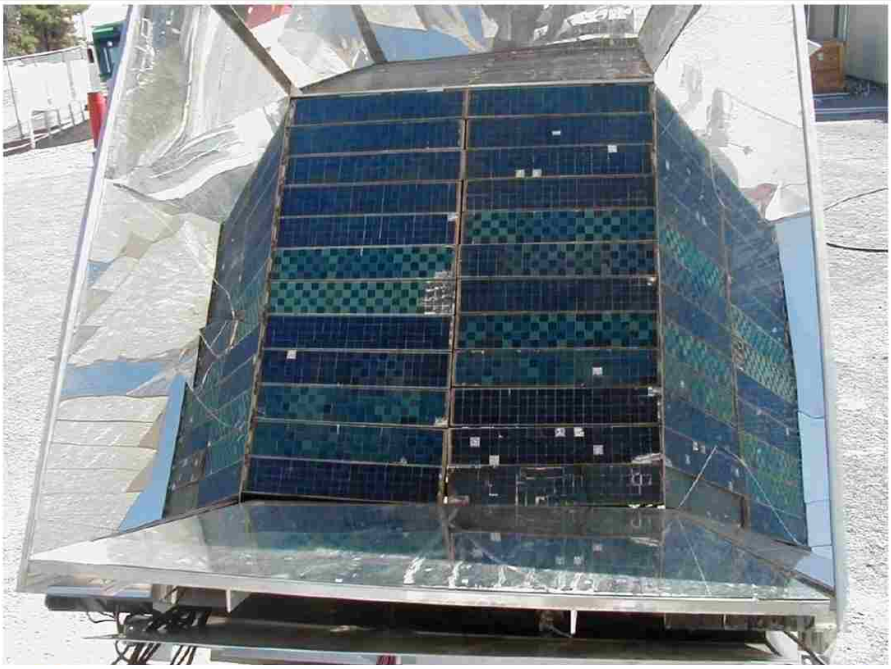

Fig. 45 The receiver area at full capacity.

Immersion of the photovoltaic cells in water will change the spectral distribution of the solar flux [20]. In calculating the inlet depth, the spectral response for the silicon cells should be first defined. In case of using deionized water the depth has a limit. This limit can be determined from Fig. 46 [34], where the relative efficiency refers to the ratio of the efficiency at any depth to the efficiency at zero depth. The

efficiency of the photovoltaic cells at any depth here is measured by the ratio of output electrical energy to the incident flux.

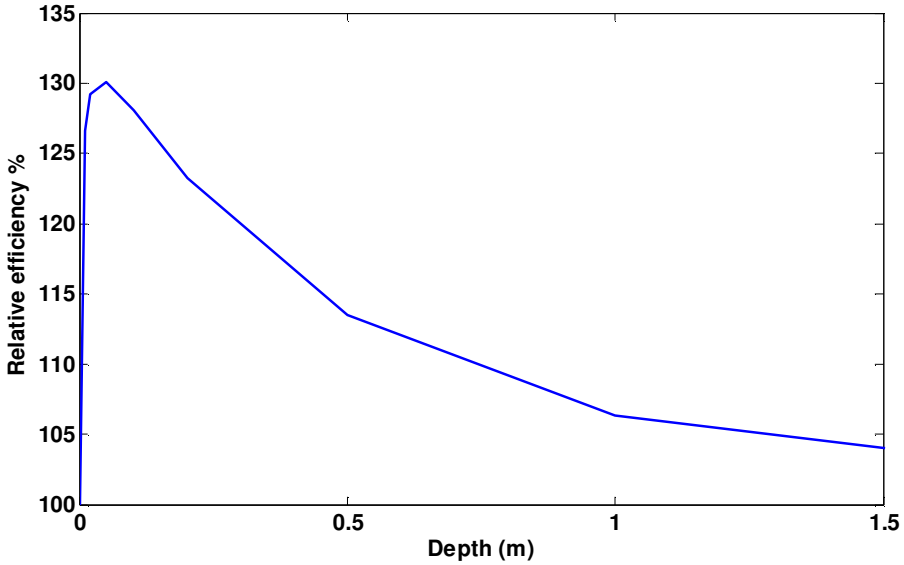

Fig. 46 Relative efficiency of the PV cell at different water depths.

In other words, immersion of the PV module under water will lead to losses. Therefore a trade off should be reached between the depth of water and the maximum available energy. From Fig. 46 we can find that the depth should not exceed 5 cm of water. Smaller heights give higher efficiencies, but more parasitic losses. Additionally smaller thickness may not provide the required cooling effect.

5.2. Cooling medium

The liquid used to cool the PV cells by an immersion technique should have good thermal, optical, and electrical properties. The coolant should have a high thermal conductivity and heat capacity, and at the same time it should have a low absorption coefficient for the solar radiation, as well be dielectric. Due to long exposure to solar radiation the coolant should also have good chemical stability.

Han et al. [39] studied different cooling media for immersion cooling of the PV cells. The properties of the coolants are summarized in Table 11.

Table 11 Summary of the coolants properties [39]

Dielectric liquid	Deionized water	Isopropyl alcohol	Ethyl acetate	Dimethyl silicon oil
Color	Clear	Clear	Clear	Clear
Refractive index	1.333	1.377	1.373	1.396
Dielectric constant	80.4	18.3	6.0	2.7
Density (kg/m^3)	1000	786	897	913
Specific heat (J/kgK)	4181	2721	1932	1550
Thermal conductivity (W/mK)	0.58	0.16	0.14	0.12
Dynamic viscosity (Pa s)	0.00089	0.0020	0.00043	0.0046
Boiling point (^oC)	100	82	77	140
Spectral transmittance	0.8002	0.803	0.8029	0.8038

The hemispherical spectral transmittance of the four liquids can be determined using the same analysis as before with the data provided in [39]. This analysis can be used to compare the performance of different coolants.

A simple comparison of the performance of the four coolants based on the cell temperature and power output at different flow rates has been performed and is represented graphically in Fig. 47 and Fig. 48.

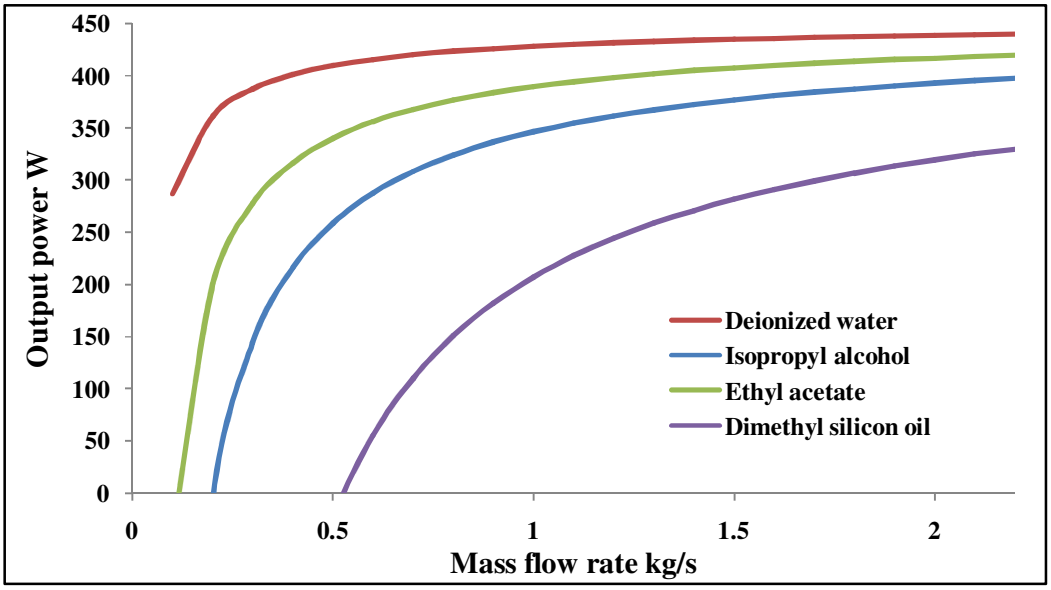

Fig. 47 Effect of coolant type on the output power

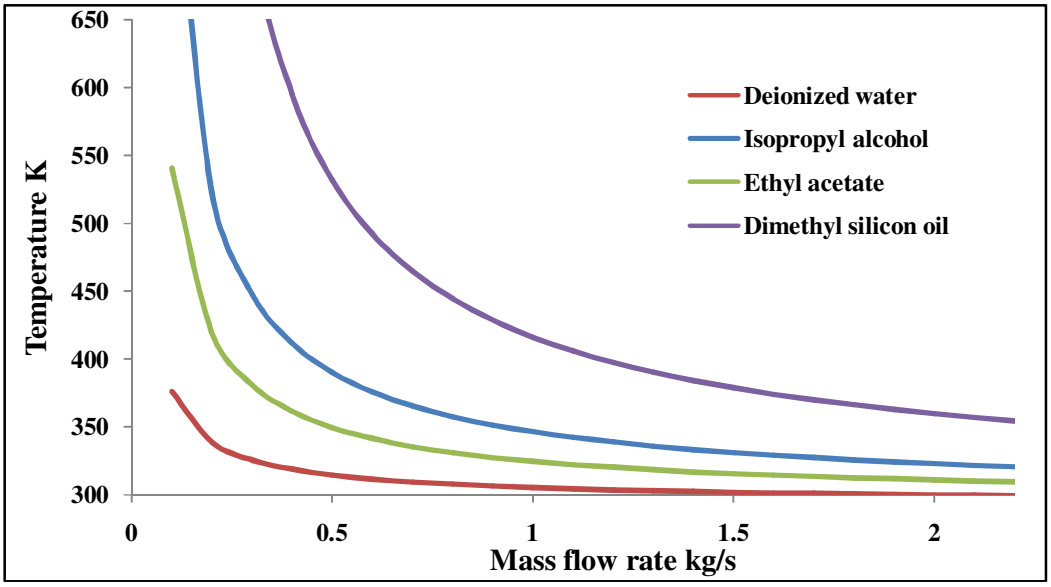

Fig. 48 Effect of coolant type on the cell temperature

The above graphs show that water is the best coolant from the thermal and optical point of view. The advantage of using silicon oil is its electric characteristics.

5.3. Concentrator design

In this experiment a concentrating dish is used to focus the solar radiation onto the PV cells. A parabolic trough with single axis tracking can be used for the same purpose as shown in Fig. 49. Normally this kind of concentrator is used with solar thermal systems where specially selected fluid is heated as it flows in a pipe.

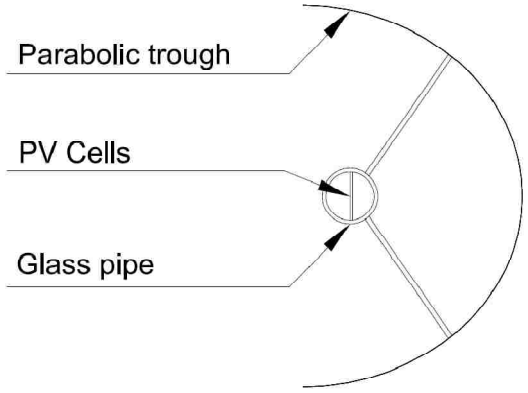

Fig. 49 Parabolic trough used with the PV cells surrounded by a coolant and transparent pipe.

The pipe geometry allows for receiving all the concentrated flux from different directions which is not the case with the flat PV cell. A different parabolic concentrator design can be used to accommodate the PV flat surface as shown in Fig. 50 [15].

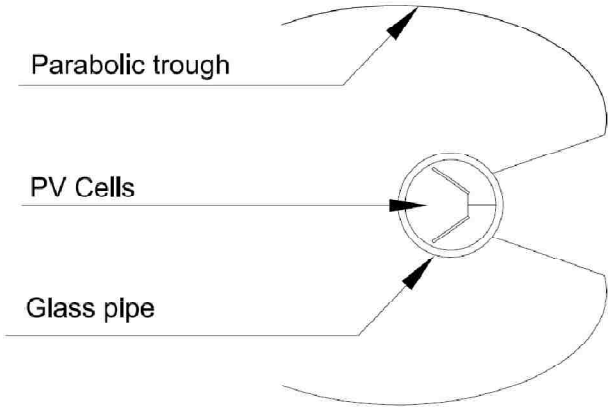

Fig. 50 Parabolic trough designed for the flat PV surface[15].

Using a parabolic trough with the PV cells opened up new ideas about a hybrid

Photovoltaic/ Thermal system (PV/T) that will be discussed in the next section.

5.4. Photovoltaic/Thermal hybrid system

The photovoltaic cells efficiency is limited by its band gap energy as discussed before. The rest of the solar energy is converted into heat. To increase the overall efficiency of the system, the concept of hybrid cycle (Photovoltaic cells / Organic Rankine Cycle) can be applied to utilize this dissipated heat. A refrigerant can be used as a working fluid in the Rankine Cycle and, R 134a has good thermal and physical properties for this application. R134a shows good electrical properties as well, when tested and used in power electronics cooling [35], [36]. The electrical properties of R-134a refrigerant are as shown in Table 12.

Table 12 Electrical properties of R134a. [37]

Medium	Resistivity (M ohms × cm)	Dissipation factor	Dielectric constant
R-134a saturated vapor 1 atm	68.18	0.0000452	1.064
R-134 vapor 1 atm	72.6	0.000459	1.0125
R-134a liquid	7400.3	1.4777	9.867

The Rankine cycle efficiency increases with the temperature while the photovoltaic cell efficiency decreases. An optimization will decide the operating temperature.

5.4.1. System overview

The photovoltaic cell array can be installed on a linear concentrator such as a trough system. The module is immersed in the cooling medium in a glass pipe as before. R134a can be used as a coolant, but the pressure is limited by the allowable pressure of the glass pipe, as a result the refrigerant pressure is low that can be inconvenient for the organic Rankine cycle.

To have a higher pressure coolant, an alternative design can be used where the module is attached to the flat side of a semicircular tube, while the refrigerant will flow inside the pipe as shown in Fig. 51. This design is different from the previous one since the cooling is from the back of the cells. The concept of cooling the back of the cells under high concentration have been studied and tested at the Center for Energy Research using the same SAIC dish. The concept was successfully applied with water as coolant. The temperature of the cells can be kept at 50˚C [20].

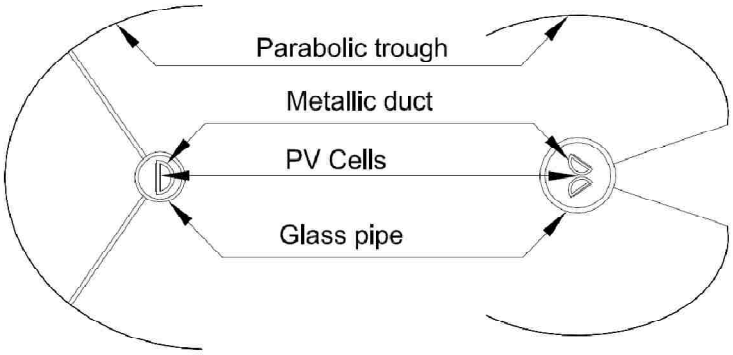

Fig. 51 PV cells cooled from the back by R 134a and enclosed in an evacuated glass pipe are shown.

The refrigerant can be used in the saturation phase. As a result, the cell temperature can be fixed at a certain value and a more uniform temperature distribution can be achieved.

The cell array and the duct can be placed in an evacuated glass tube to reduce the radiation and the convection losses to the environment.

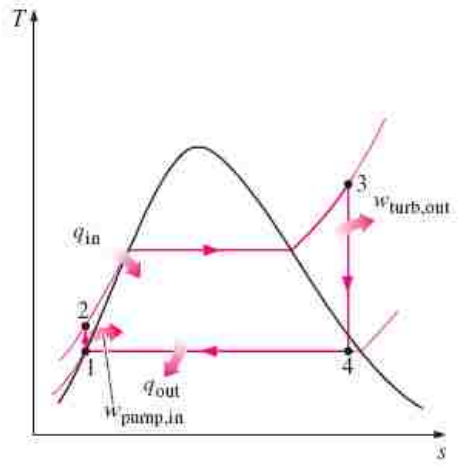

Fig. 52 An ideal Rankine cycle is shown and analyzed below [38].

5.4.2. System analysis

A Rankine cycle consists of four processes as noted in the following [38]:

1-2 Pumping the working fluid where the pumping power

$$w_{pump} = h_2 - h_1 \quad 5\text{-}1$$

2-3 Heat addition in the parabolic trough

$$q_{in} = h_3 - h_2 \quad 5\text{-}2$$

3-4 Working fluid expansion in the turbine

$$w_{turbine} = h_3 - h_4 \quad 5\text{-}3$$

4-1 Heat rejection in the condenser

$$q_{out} = h_4 - h_1 \quad 5\text{-}4$$

The cycle efficiency is:

$$\eta_{cycle} = \frac{w_{net}}{q_{in}} = 1 - \frac{q_{out}}{q_{in}} \quad 5\text{-}5$$

At the steady state conditions, using the energy conservation equation, the mass flow rate of the coolant can be determined as follows:

$$\dot{m}_C q_{in} = X H_b A_{pv}(1 - \eta_{pv}) \qquad 5\text{-}6$$

where the absorbed energy by the coolant is equal to the total concentrated solar radiation minus the solar energy converted by the cell into electricity.

The photovoltaic cells efficiency generally can be expressed in the following form [5]:

$$\eta_{pv} = a[1 - b\, T_{pv}] \qquad 5\text{-}7$$

The cells under discussion have the following efficiency-temperature relationship:

$$\eta_{pv} = \eta_{T_{ref}}[1 - 0.0045(T_{pv} - 25)] \qquad 5\text{-}8$$

Where the highest temperature in the cycle is determined by the photovoltaic cell temperature and the lowest temperature can be the ambient temperature. The overall system efficiency can be found as follows:

$$\eta_{overall} = \frac{DNI \times \eta_{pv} + DNI \times (1 - \eta_{pv}) \times \eta_{cycle}}{DNI} \qquad 5\text{-}9$$

$$\eta_{overall} = \eta_{pv} + \eta_{cycle} - \eta_{pv}\, \eta_{cycle} \qquad 5\text{-}10$$

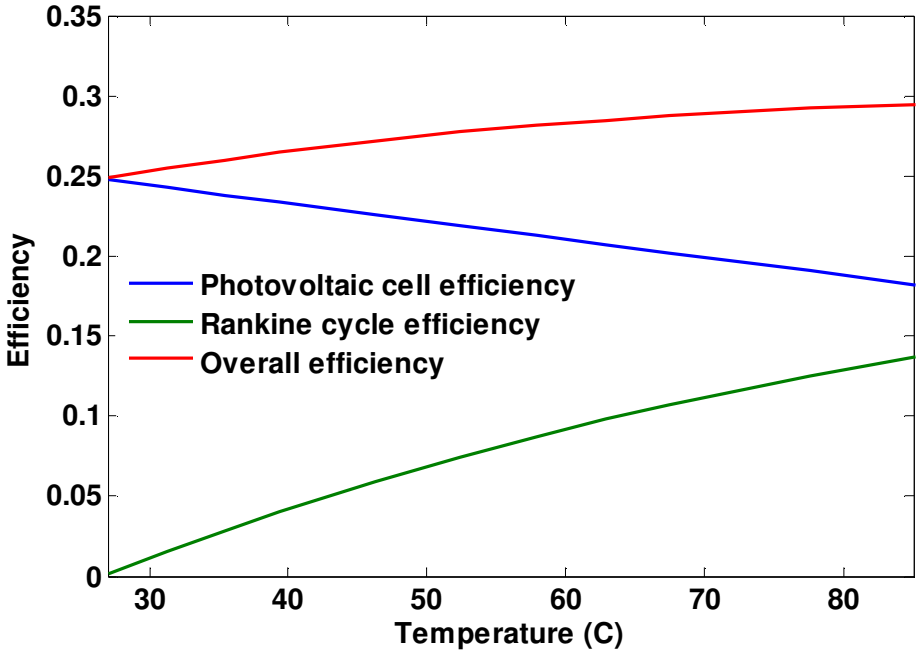

Fig. 53 PV/T hybrid system efficiency.

The overall system efficiency will increase, but the optimum operating temperature shouldn't exceed the allowable temperature for the PV cell.

CHAPTER 6

6. CONCLUSIONS

Immersion cooling technique is capable of attaining low, uniform temperatures along a PV array surface. Lower temperatures can be achieved using the immersion technique than the back-of-the-cell cooling technique. In the experiment the module temperature uniformity can be increased by applying the flow of the cooling medium along the short edge of the PV cell surface. Water is the most efficient coolant considered here, but it requires additional sophistication in terms of deionization processing. More research work should be carried out to find a dielectric cooling medium with similar thermal properties as water. Also, there are many practical issues that need to be worked out related to the PV receiver design for both economical and efficient application on large scale.

APPENDIX A
NOMENCLATURE

A	Area, m^2	σ	Stefan-Boltzmann constant W/m^2K^4
a	Junction area m^2	τ	Transmissivity
a_1, b_1	Constants	η	Efficiency
A_{total}	Total absorptance	μ	Dynamic viscosity $N.s/m^2$
A_r	Absorptance for single ray	$\hbar$	Planck's constant, eVs
C_p	Heat capacity, kJ/kg K	ω	Frequency, 1/s
D	Diameter, m, Diffusion coefficient cm^2/s	Subscripts	
E	Electrical power, W	A	Acceptor
e	Elementary charge, As	Abs	Absorbed
FF	Fill factor	B	Beam radiation
G_T	Total solar radiation flux, W/m^2	C	Cell
G	Generation rate, $1/cm^3$ s	D	Diameter, Donor
H	Component of solar radiation, W/m^2	D	Diffuse radiation
h	Convection heat transfer coefficient, W/m^2K	E	Electron
j	Charge current density, $1/cm^2$	Ext	External
k	Thermal conductivity, W/mK, Boltzmann's constant, eV/K	f.c.	Forced convection
L	Diffusion length, cm	G	Glass
M	Concentration ratio	H	Hydraulic, Hole
$\dot{m}$	Mass flow rate, kg/s	I	Inlet, Intrinsic
Nu	Nusselt number	In	Intermediate
n	Refractive index, Concentration of electrons, holes	inc	Incident
Pr	Prantdl number	Int	Internal
Q	Heat flow, W	M	Mean bulk
R_{total}	Total reflectance	max	Maximum
R_r	Ray reflectance	MP	Maximum power
Re	Reynolds number	n.c.	Natural convection
r	Radius, m	O	Out
r_s	Internal series resistance, Ohm	Oc	Open circuit
T	Temperature, K	P	Copper plate
T_{total}	Total transmittance	Pro	Projected area
Tr	Ray Transmittance	pv	Photovoltaic cell
t	Thickness, m	Q	Electrical current
V	Ambient air velocity, m/s, Voltage, V	R	Radiation heat transfer

Greek		ref	Reference
κ	Absorption coefficient, cm^{-1}	S	Saturation
λ	Wave length, μm	Sc	Short circuit
ρ	Reflectivity	total	Total
ϕ	Longitudinal angle	W	Water
θ	Angle	DC	Direct current
α	Absorptivity	∞	Ambient
ε	Emissivity, Energy of electron, hole, eV		

REFERENCES

[1] Peter Wurfel, Physics of solar cells, Wiley-Vch, 2005.

[2] D. J. Mbewe, H. C. Card and D. C. Card, A model of silicon solar cells for concentrator photovoltaic and photovoltaic thermal system design, Solar energy vol. 35, No. 3, pp. 247-258, 1985.

[3] G. Sala, Solar cells and optics for photovoltaic concentration, Adam Hilger, Bristol and Philadelphia, 1989, pp. 239–267.

[4] M.J. O'Leary and L.D. Clements, Thermal-electric performance analysis for actively cooled, concentrating photovoltaic systems, Sol. Energy 25 (1980), pp. 401–406.

[5] Anja Royne, and Christopher J. Dey, Cooling of photovoltaic cells under concentrated illumination: a critical review, Solar energy materials & solar cells 86 (2005) 451–483.

[6] R.A. Sinton, Y. Kwark, P. Gruenbaum and R.M. Swanson, Silicon point contact concentrator solar cells, Conference record, 18th IEEE PVSC, 1985, pp. 61–65.

[7] V.L. Dalal and A.R. Moore, Design considerations for high-intensity solar cells, J. Appl. Phys. 48 (1977) (3), pp. 1244–1251

[8] A. Luque, G. Sala and J.C. Arboiro, Electric and thermal model for non-uniformly illuminated concentration cells, Sol.Energy Mater. Sol. Cells 51 (1998), pp. 269–290.

[9] R.K. Mathur, D.R. Mehrotra, S. Mittal and S.R. Dhariwal, Thermal non-uniformities in concentrator solar cells, Sol. Cells 11 (1984), pp. 175–188.

[10] F. Chenlo and M. Cid, A linear concentrator photovoltaic module: analysis of non-uniform illumination and temperature effects on efficiency, Sol. Cells 20 (1987), pp. 27–39.

[11] Yu.A. Abrahamyan, The efficiency of solar cells immersed in liquid dielectrics, Solar energy materials & Solar cells 73 (2002) 367–375.

[12] Yiping Wang, Zhenlei Fang, The performance of silicon solar cells operated in liquid, Applied energy 86 (2009) 1037–1042.

[13] Li Zhu, YipingWang, An effective heat dissipation method for densely packed solar cells under high concentration, Solar energy materials & solar cells 94 (2010) 133–140.

[14] Anja Royne , Christopher J. Dey, Design of a jet impingement cooling device for densely packed PV cells under high concentration, Solar energy 81 (2007) 1014–1024.

[15] A. Akbarzadeh and T. Wadowski, Heat pipe-based cooling system for photovoltaic cells under concentrated solar radiation, Applied thermal engineering Vol. 16, No. 1, pp. 81-87, 1996.

[16] J.B. Lasich, Cooling circuit for receiver of solar radiation, Patent WO02080286, 2002, Australia.

[17] P.J. Verlinden, A. Terao, D.D. Smith, K. Mcintosh, R.M. Swanson, G. Ganakas and J.B. Lasich, Will we have a 20%-efficient (PTC) photovoltaic system?

Conference record, Proceedings 17th European PhotovoltaicSolar Energy Conference, 2001.
[18] C. L. Tilford, R. A. Sinton, R. M. Swanson, R. A. Crane and P. Verlinden, Development of a 10 kW reflective dish PV system, Conference record, 23rd IEEE PVSC, 1993, pp. 1222–1227.

[19] M.A. Newmarker, Development and testing of an advanced photovoltaic receiver, Dissertation, Department of mechanical engineering, University of Nevada Las Vegas, 2007.
[20] -- SAIC Concentrating Dish/PV System Development final report to NREL from the UNLV Center for Energy Research, June 18, 2007.
[21] Li Zhu and Robert F Boehm, Water immersion cooling of PV cells in a high concentration system, Solar energy materials & solar cells 95 (2011) 538–545.
[22] K. Tanaka, Solar energy converter using a solar cell in a shallow liquid layer, Patent US6583349B2, 2003.
[23] K. Tanaka, Solar energy converter using a solar cell in a shallow liquid-gel layer, Patent US7244888B1, 2007.
[24] A. Royne and C.J. Dey, Design of a jet impingement cooling device for densely packed PV cells under high concentration, Solar energy 81 (2007), pp. 1014–1024
[25] H.C. Koehler, Cooling photovoltaic (PV) cells during concentrated solar radiation in specified arrangement in coolant with as low electric conductivity as possible, Patent DE19904717, 2000.
[26] O.V. Vasilinina, J.K. Kidyashev, V.N. Potapov, S.V. Ryabikov, A.M. Stepanov and D.S. Strebkov, Solar photoelectric conversion apparatus with cooling means, Patent US4211581, 1980.
[27] L. Zhu, Y.P. Wang, Z.Y. Zhang, Z.L. Fang and Y. Fang, Study the weather-resistance of dimethyl polysiloxane used in liquid-immersing CPV receivers, Acta Energiae Solaris Sinica 31 (2010), pp. 191–196.
[28] Tai-Hsi Fan and Andrei G. Fedorov, Radiative transfer in a semitransparent hemispherical shell, Journal of quantitative spectroscopy & radiative transfer 73 (2002), pp. 285–296.
[29] R. Seigel and J. Howell, Thermal radiation heat transfer, fourth edition, Hemisphere Publishing Corporation, 2002.
[30] C. K. Hsieh, Thermal analysis of CPC collectors, Solar energy 27 (1981), pp. 19–29.
[31] F. Incropera and D. Dewitt, Fundamentals of heat and mass transfer, fifth edition, John Wiley Publishing, 2009.
[32] E. Skoplaki and J.A. Palyvos, On the temperature dependence of photovoltaic module electrical performance: A review of efficiency/power correlation, Solar Energy 83 (2009), pp. 614–624.
[33] A, J. Chapman, Heat Transfer. 3rd Ed., MacMillan, New York (1974).
[34] J. A. Muaddi and M. A. Jamal , Spectral response and efficiency of a silicon solar cell below water surface, Solar energy vol. 49, No. 1, pp. 29-33, 1992.

[35] Mitch Olszewski , Potential refrigerants for power electronics cooling, NREL, 2005

[36] Jeremy B. Campbell, Two-phase cooling method using the R134a refrigerant to Cool power electronic devices, IEEE transaction on industrial applications, vol. 43, no. 3, May/June 2007

[37] Andrew M. Gubr and John J.Byme, Determination of dielectric properties of refrigerants, ASHRE research project 1074-RP, 2001.

[38] Yunus A. Cengel and Michael A. Boles, Thermodynamic an engineering approach, fifth edition, McGraw-Hill, 2005

[39] Xinyue Han, Yiping Wang, and Li Zhu, Electrical and thermal performance of silicon concentrator solar immersed in dielectric liquids, Applied energy xxx (2011) xxx–xxx.

VITA

Graduate College
University of Nevada, Las Vegas
Ahmed Darwish

Degree:

Bachelor of Science, Mechanical Engineering, 2005
Al Azhar university, Cairo, Egypt

Thesis Title: Immersion Cooling of Photovoltaic Cells in Highly Concentrated Solar Beams

Selected Publications:

Ahmed Darwish, Robert Boehm, Optical and thermal analysis for immersed cooling of photovoltaic cells in a highly concentrated beam, ASME 2011 5th International Conference on Energy Sustainability, 2011.

Ahmed Darwish, Robert Boehm, Compressed air energy storage flow and power analysis, ASME 2011 5th International Conference on Energy Sustainability, 2011.

Thesis Examination Committee:

Chairperson, Dr. Robert Boehm, PH. D.
Committee Member, Dr. Yitung Chen, PH. D.
Committee Member, Dr. Suresh B. Sadineni, PH. D.
Graduate Faculty Representative, Dr. Aly Said, PH. D.